

## Article

# Interdecadal Changes of the MERRA-2 Incoming Surface Solar Radiation (SSR) and Evaluation against GEBA & BSRN Stations

Michael Stamatis <sup>1</sup>, Nikolaos Hatzianastassiou <sup>1,\*</sup>, Marios Bruno Korras-Carraca <sup>1,2</sup>, Christos Matsoukas <sup>2</sup>,  
Martin Wild <sup>3</sup> and Ilias Vardavas <sup>4</sup>

<sup>1</sup> Laboratory of Meteorology & Climatology, Department of Physics, University of Ioannina, 45110 Ioannina, Greece

<sup>2</sup> Department of Environment, University of the Aegean, 81100 Mytilene, Greece

<sup>3</sup> Institute for Atmospheric and Climate Science, ETH Zürich, 8092 Zürich, Switzerland

<sup>4</sup> Department of Physics, University of Crete, 71003 Heraklion, Greece

\* Correspondence: nhatzian@uoi.gr

**Abstract:** This study assesses and evaluates the 40-year (1980–2019) Modern-Era Retrospective Analysis for Research and Applications v.2 (MERRA-2) surface solar radiation (SSR) as well as its interdecadal changes ( $\Delta(\text{SSR})$ ) against high quality reference surface measurements from 1397 Global Energy Balance Archive (GEBA) and 73 Baseline Surface Radiation Network (BSRN) stations. The study is innovative since MERRA-2 ( $\Delta(\text{SSR})$ ) has never been evaluated in the past, while the MERRA-2 SSR fluxes themselves have not been evaluated in such large spatial scale, which is global here, and temporal basis, which counts 40-years. Other novelties of the study are the use of the highest quality BSRN stations, done for the first time in such an evaluation, as well as the use of a greater number of reference-GEBA stations than in other studies. Moreover, the assessment and evaluation in this study are largely based on SSR anomalies, while being done in depth, at spatial scales ranging from the local to global/hemispherical, and separately for land and ocean areas, and at temporal scales spanning intervals from decadal sub-periods to 40 years. Overall, the MERRA-2 deseasonalized SSR anomalies correlate well with either GEBA (R equal to 0.61) and BSRN (R equal to 0.62). The percentage of agreement between the sign of computed GEBA and MERRA-2  $\Delta(\text{SSR})$  is equal to 63.4% and the corresponding percentage for MERRA-2 and BSRN is 50%. According to MERRA-2, strong and statistically significant positive  $\Delta(\text{SSR})$  (Brightening) is found over Europe, Central Africa, Mongolia, Mexico, Brazil, Argentina and some parts of the tropical oceans. In contrast, large and statistically significant negative  $\Delta(\text{SSR})$  (Dimming) occurs over the western Tropical Warm Pool, India, Southern East China, Amazonia, stratocumulus covered areas and some parts of oceans. MERRA-2 yields a dimming equal to  $-0.158 \pm 0.005 \text{ W/m}^2/\text{year}$  over the globe from 1980 to 2019. This 40-year dimming, which occurred in both hemispheres, more over ocean than continental areas ( $-0.195 \pm 0.006$  and  $-0.064 \pm 0.006 \text{ W/m}^2/\text{year}$ , respectively), underwent decadal scale variations.

**Keywords:** surface solar radiation; climate; dimming; brightening; model; stations; reanalysis



**Citation:** Stamatis, M.; Hatzianastassiou, N.; Korras-Carraca, M.B.; Matsoukas, C.; Wild, M.; Vardavas, I. Interdecadal Changes of the MERRA-2 Incoming Surface Solar Radiation (SSR) and Evaluation against GEBA & BSRN Stations. *Appl. Sci.* **2022**, *12*, 10176. <https://doi.org/10.3390/app121910176>

Academic Editors: Harry D. Kambezidis and Basil Psiloglou

Received: 31 August 2022

Accepted: 5 October 2022

Published: 10 October 2022

**Publisher's Note:** MDPI stays neutral with regard to jurisdictional claims in published maps and institutional affiliations.



**Copyright:** © 2022 by the authors. Licensee MDPI, Basel, Switzerland. This article is an open access article distributed under the terms and conditions of the Creative Commons Attribution (CC BY) license (<https://creativecommons.org/licenses/by/4.0/>).

## 1. Introduction

Solar radiation is the main energy source for the Earth-atmosphere system, while the incoming surface solar radiation (SSR) at the Earth's surface plays an important role for various biological, physical and chemical processes, being strongly related to climate and its changes [1,2]. SSR is driven either by astronomical factors, such as the Sun–Earth distance, the solar zenith angle and position (latitude) or by the composition of the atmosphere, surface conditions, and human activities [3,4]. As a result, and based on the combination of all these factors, great spatiotemporal changes in the SSR are created. These changes have strengthened the interest of the scientific community due to possible implications for global climate change, but also the steadily increasing use of solar energy [5–7]. The interdecadal

increases or decreases of SSR, commonly known as global dimming and brightening (GDB), started to gain recognition in the late 1980s [8,9]. GDB may be a regional or global phenomenon and it has been proven that its two major drivers are clouds and aerosols, which largely determine the transparency of the atmosphere [10–12]. GDB has implications for various sectors ranging from economy, solar power, hydrology and agriculture to climate. The growth of plants and the yield of crops depend on sunshine that creates photosynthesis, but also on temperature, which is strongly dependent on SSR [13–15]. For example, the increasing diffuse radiation, occurring during dimming phases due to increasing air pollution and cloudiness, enhances photosynthesis in tall vegetation, while low vegetation does not benefit so much [16]. GDB affects the hydrological cycle [17] and changes the diurnal range of surface temperature. Yet, probably the most important effect of GDB is on climate. Thus, [18] noticed that since the 1980s, the lack of solar dimming and its masking effects, allowed the warming by greenhouse gases to become more obvious, resulting in a more rapid increase of temperature than in previous decades.

Because of its various and important effects, GDB has become a significant topic of international research, being investigated using either observations and measurements or modelling tools. Direct measurements of SSR have the advantage of providing higher accuracy, but smaller spatial representativeness, while satellite- and model-based products, or combined products, ensure a great representativeness, but need to be evaluated against ground-based truth. Initially, ground-based observations of SSR over North America and Europe have shown a negative trend from the 1960s to the 1980s, referred as ‘dimming’ [10,19–22], and a positive trend, i.e., a ‘brightening’, from the middle 1980s through to 2000 [5,11,23,24]. However, solar dimming continued to exist until 2000 over India and Southeast Asia [25–28]. Beyond 2000, it was found that the brightening continued over Europe and N. America and levelled-off at sites in Japan, while in India and China there was a dimming [5]. Besides, it has been suggested [22] that the greenhouse warming after 2000 may be less modulated by GDB than in previous decades, which may be considered in relation to the recent global warming hiatus observed at the beginning of the 21st century [29–31]. The GDB results from studies based on surface measurements are complemented by others obtained using satellite observations and models, which provide the necessary spatial coverage and representativeness. Thus, GDB results obtained on regional/global scale, using model simulations and/or satellite data [10,12,32–38], provided evidence that the dimming and brightening during the 1980s and 1990s, respectively, were global rather than local, but also reported contrasting trends in SSR even over neighboring regions. During 1984–2000, significant increasing trends in SSR, equal to  $2.4 \text{ Wm}^{-2}\text{decade}^{-1}$ , were found in the International Satellite Cloud Climatology Project–D2 series (ISCCP-D2) satellite-based analysis by [10]. Furthermore, a global solar brightening of  $1.6 \text{ Wm}^{-2}\text{decade}^{-1}$  between 1983 and 2001 has been estimated by [35] using satellite retrievals (ISCCP-D1), associated with a decrease of clouds. The assessment made by [36] using Global Energy and Water Exchanges Project–Surface Radiation Budget version 2.8 (GEWEX-SRB V2.8) data, revealed a dimming equal to  $2.51 \text{ Wm}^{-2}\text{decade}^{-1}$  between 1983 and 1991, followed by a brightening of  $3.17 \text{ Wm}^{-2}\text{decade}^{-1}$  from 1991 to 1999, and then a subsequent dimming of  $5.26 \text{ Wm}^{-2}\text{decade}^{-1}$  during 1999–2004, yielding an overall global brightening of  $0.25 \text{ Wm}^{-2}\text{decade}^{-1}$  during 1983–2004. An overall dimming of  $-2.0 \text{ Wm}^{-2}$  from 1920 to 2000 has been computed by [32] that was consistent with the simulations from 10 models implemented in United Nations Intergovernmental Panel on Climate Change—Fourth Assessment Report (IPCC-AR4) that show a global dimming of  $-1$  to  $-4 \text{ Wm}^{-2}$  during the 20th century. They also found dimming from 1968 to 1977 followed by brightening during the 1980s and 1990s. Also, a study by [34] using a radiation transfer model with input ISCCP-D2 satellite data for the period 2000–2007 found a solar dimming in the Southern Hemisphere, due to increasing aerosols and clouds, but without a clear signal of dimming or brightening in the Northern Hemisphere, where a dimming was mostly observed over the oceans and a slight brightening over land. Slightly extending the study period, through to 2009, the same authors [12] found again a stronger

dimming in the Southern Hemisphere along with a smaller dimming in the Northern Hemisphere. Moreover, a brightening equal to  $+0.03 \text{ Wm}^{-2}\text{decade}^{-1}$  has been estimated by [37] using retrieved Clouds and the Earth's Radiant Energy System (CERES) satellite SSR data for the period 2001–2012. The same authors using ISCCP-FD SSR data estimated a stronger dimming of  $-5.05 \text{ Wm}^{-2}\text{decade}^{-1}$  during 2000–2009 and a weaker dimming of  $-1.15 \text{ Wm}^{-2}\text{decade}^{-1}$  during 1984–2009. All these results highlight the complex nature of GDB patterns in terms of spatial and temporal variability. Contrasting signs of SSR trends appear over adjacent areas, whereas the sign of GDB is sensitive to the selected study period, possibly changing by extending the study period by a few years, especially when relatively short periods are assessed. All these complexities point to the need for assessing GDB over as long as possible time periods and utilizing homogeneous SSR data sets.

Reanalysis SSR products, that combine observations with models, have the advantage of providing full spatial coverage and long temporal coverage and therefore have been widely used in the atmospheric sciences and climate change studies [39]. Some of the reanalysis products are: the NCEP-NCAR, NCEP-DOE and Climate Forecast System Reanalysis (CFSR) from National Centers for Environmental Prediction and National Center for Atmospheric Research (NCEP) [40]; ERA-5, which replaced the ERA-Interim from European Centre for Medium-Range Weather Forecasts (ECMWF) [41]; the JRA-55 from Japan Meteorological Agency (JMA) [42]; the National Oceanic and Atmospheric Administration (NOAA)–CIRES–DOE 20th Century Reanalysis V3 [43] and the Modern-Era Retrospective Analysis for Research and Applications, Version 2 (MERRA-2) reanalysis of the National Aeronautics and Space Administration (NASA) Goddard Space Flight Center (GSFC)'s Global Modeling and Assimilation Office (GMAO). Products from these Reanalyses have been used to provide climatological assessments of SSR. Thus, [44] reported that over the period January 2001–December 2015 the mean global surface solar radiation from MERRA-2 is equal to  $185.6 \text{ Wm}^{-2}$ , while for the same period, according to [45], JRA-55 yields  $189 \text{ Wm}^{-2}$ , ERA5  $187.9 \text{ Wm}^{-2}$ , NOAA–CIRES–DOE gives  $192.9 \text{ Wm}^{-2}$  and from NCEP-NCARSSR is equal to  $205.3 \text{ Wm}^{-2}$ . Nevertheless, land surface data obtained from reanalyses have problems caused by inhomogeneities in the assimilated data records that obtained primarily from atmospheric profiles, affecting the near-surface meteorology. These errors, along with others, like those related to clouds, aerosols, water vapor, topography and surface albedo, can cause systematic biases in reanalysis SSR products [39,46]. Indeed, most reanalyses (including MERRA and MERRA-2) showed average positive biases [39,47], and a strong overestimation of SSR over regions such as Europe, Asia and North America. This positive bias was found to be due to an underestimation of the cloud fraction [39,48]. In addition, the study by [49] revealed that MERRA and ERA-Interim reanalyses often predict clear sky conditions, while actual conditions are cloudy, yielding an overestimation of SSR, with the opposite, namely actual clear-sky conditions predicted by reanalyses as cloudy, yielding an underestimation of SSR, being less pronounced. The same finding was reported by [50] over the tropical Atlantic Ocean using MERRA-2 and ERA-5. Hence, there is a systematic effort to produce Reanalyses with improved quality products, e.g., MERRA-2 versus MERRA. Thus, [44] showed that MERRA-2 SSR represent better than MERRA the variability and trends in the global mean radiative fluxes over the period 2001–2015, however noting that the MERRA-2 radiative fluxes themselves are not clearly better than the MERRA ones, since both improvements and deterioration were found. Also, the same study proved that clouds are clearly a source of significant SSR errors in both MERRA and MERRA-2. Of course, these SSR uncertainties also make any Reanalysis-based GDB assessment uncertain. Therefore, it is evident that a thorough validation of not only the reanalysis SSR products, but also the associated SSR trends and GDB, against available reference ground measurements is necessary before being used in climate studies. Such evaluations have been made only for reanalysis SSR, and much less for SSR trends, as well as for its driving factors. Most studies have performed reanalyses' SSR evaluation against ground-based stations over several regions, such as Indonesia [51], Balochistan (Pakistan, [52]), Europe [53], Norway [54], East Antarctic Plateau [55], Yangtze River Delta [56],

China [47] and references therein, East Asia [46], North America [57], Ireland [58], South Africa [59], Ehtioipian Highlands [60], and Eurasia [61]. Besides, the ERA40 reanalysis SSR has been evaluated globally against ground-based GEBA (Global Energy Balance Archive) stations [62], the ERA5 and MERRA-2 SSR were evaluated against BSRN (Baseline Surface Radiation Network) stations [63], while the ERA-Interim, JRA-55 and NCEP-DOE SSR were validated against GEBA and CMA (China Meteorological Administration) stations [64].

Much fewer studies deal with the assessment even fewer with the evaluation of SSR trends. The study by [38] evaluated the SSR of MERRA-2 reanalysis against ground-based (GEBA and CMA) stations. For regions over which good SSR evaluation metrics, they also investigated the SSR long-term trends from 1980 to 2019 and estimated and examined the corresponding trends of clouds and aerosols. They found that during 1980–2019, there has been a widespread decline of SSR (dimming) in North America, Northeast Asia and Oceania, equal to  $-0.32$ ,  $-0.00$  and  $-1.14 \text{ Wm}^{-2}\text{decade}^{-1}$ , respectively, and an increase of  $0.63 \text{ Wm}^{-2}\text{decade}^{-1}$  over Europe. Apart from this study, which investigated but not evaluated the MERRA-2 SSR trends, the interdecadal variation of various reanalysis SSR was computed and evaluated against ground-based stations over specific world regions, such as China (MERRA-2 by [65]; ERA5 by [66]; ERA-Interim and MERRA by [67]; NCEP/NCAR, NCEP/DOE and MERRA-2 by [68]), the Tibetan Plateau (NCEP/NCAR and ERA-40 by [69]), the Iberian Peninsula (ERA-40 by [70]), the Euro-Mediterranean region (ERA5 by [71]), Brazil (ERA5, MERRA-2, JRA55 and CFSR by [72]) and Europe (20CRv2c, 20CRv3, ERA20C and CERA20C by [73]) or globally (ERA5 by [74]; ERA40 by [62]).

Most of the previous studies evaluated SSR products of various reanalyses using a limited number of observations and for selected regions of our planet. In addition, fewer studies evaluated the reanalysis SSR, on a seasonal and regional basis [38,39]. Even fewer studies have done so for SSR trends. Actually, no evaluation of MERRA-2 SSR trends, i.e., GDB, especially at global scale, has been made to date. This is attempted, for the first time to our knowledge, in the present study, which evaluates the 40-year (1980–2019) GDB based on MERRA version 2 (MERRA-2), the latest and improved available version of MERRA. Apart from the MERRA-2 SSR changes, the present study also thoroughly evaluates the MERRA-2 SSR over the 40-year period 1980–2019 against SSR measurements from two top-quality ground-based reference networks of stations distributed all over the globe, namely GEBA and the BSRN. It should be noted that apart from the novelty of providing a first-seen detailed evaluation of MERRA-2 Reanalysis GDB, the present study also has the originality of validating the MERRA-2 SSR fluxes against the absolute reference network of BSRN stations, apart from GEBA, whereas similar evaluation of MERRA-2 SSR has been done in the past only against GEBA [38]. Here, the parallel use of SSR measurements from both BSRN, which ensures the best reliability, and GEBA, which provides wider spatial coverage than BSRN, allows the derivation of more robust conclusions about the quality of MERRA-2 Reanalysis SSR and GDB. Moreover, in order to further strengthen the robustness of the derived conclusions and to achieve the maximum possible reliability of the computed MERRA-2 GDB, a columnar closure study was undertaken, in which the long-term changes of MERRA-2 reflected solar radiation fluxes at the Top of Atmosphere (TOA) were compared to the corresponding trends of TOA reflected solar radiation fluxes of CERES-EBAF, used as reference. The evaluation of MERRA-2 SSR and GDB is done using deseasonalized anomalies at various scales, ranging from the local (station-level) to global/hemispherical ones, and for temporal scales ranging from the entire 40-year study down to selected specific sub-periods. Section 2 describes the utilized data and the applied methodology, Section 3 presents and discusses the results of the attempted evaluation and finally the conclusions are drawn in Section 4.



## 2. Materials and Methods

### 2.1. Data

#### 2.1.1. MERRA-2

MERRA-2 is a global atmospheric reanalysis produced by the NASA Global Modeling and Assimilation Office (GMAO) in 2017 [75]. It provides data beginning in 1980, with continuous updates, having high spatial ( $0.5^\circ$  latitude  $\times$   $0.625^\circ$  longitude and 72 hybrid sigma-pressure layers from the surface to 0.01 hPa) and temporal (hourly) resolution, that is freely available at [76]. The goals of MERRA-2 are to provide a regularly gridded, homogeneous record of the global atmosphere, climate system and improved land surface representation and cryospheric processes. MERRA-2 is the first long-term satellite-era global reanalysis to assimilate space-based observations of aerosols, representing their interactions with other physical parameters in the climate system. It was introduced to replace the original MERRA product and reflects recent advances in atmospheric modeling and data assimilation, namely assimilation of modern hyperspectral radiance and microwave observations, along with GPS-Radio Occultation datasets, use of NASA's ozone profile observations that began in late 2004, as well as additional advances in both the GEOS model and the GSI assimilation system [77]. More specifically, the MERRA-2 SSR fluxes are utilized in the present study, computed by the shortwave radiation parameterization described by [78]. This parameterization scheme resolves the absorption by water vapor, oxygen, ozone, carbon dioxide, and aerosols, while the SSR fluxes are integrated virtually over the entire solar spectrum, from  $0.175 \mu\text{m}$  to  $10 \mu\text{m}$ . In the ultraviolet and visible regions, the spectrum is divided into 8 bands, and single ozone absorption coefficient and Rayleigh scattering coefficient are used for each band. In the infrared, the spectrum is divided into 3 bands, and the k-distribution method is applied for water vapor absorption. For each one of the 72 atmospheric layers, transmissivity and reflectivity are first calculated using the  $\delta$ -Eddington approximation [79], while spectral fluxes are then calculated using the two-stream adding method for the composite layers. The total SSR flux at each pressure level and at the Earth's surface is the weighted (by the fraction of extraterrestrial solar flux contained in the above-mentioned bands) sum of these fluxes. For the aim of this study monthly MERRA-2 SSR fluxes, called "SWGDN", are utilized.

#### 2.1.2. CERES-EBAF

The Clouds and the Earth's Radiant Energy System—Energy Balanced and Filled (CERES-EBAF) product provides 1-degree latitude-longitude global monthly mean shortwave, longwave and net fluxes, at the Top-of-Atmosphere and at the Earth's surface, under clear and all-sky conditions. CERES instruments are onboard the Terra, Aqua, Suomi National Polar-Orbiting Partnership (SNPP) and NOAA-20 satellites. Each instrument measures filtered radiances in the shortwave (between  $0.3$  and  $5 \mu\text{m}$ ), total (between  $0.3$  and  $200 \mu\text{m}$ ), and window (between  $8$  and  $12 \mu\text{m}$ ) regions [80]. The filtered radiances are transformed to unfiltered shortwave, longwave and window radiances following the [81] scheme, which then are converted to instantaneous TOA radiative fluxes using empirical angular distribution models [82]. These instantaneous TOA fluxes are spatially averaged on a  $1^\circ$  equal-area grid and interpolated between observed values at 1-h increments for each hour in coordinated universal time (UTC) of every month, and finally averaged over all hour boxes in a month [83]. CERES-EBAF data span the period from March 2000 to the present and produce a long-term, integrated global climate data record for detecting decadal changes in the Earth's Radiation Budget from the surface to the Top of Atmosphere together with the associated cloud and aerosol properties. Here we use the EBAF Edition 4.1 level 3b Top of The Atmosphere monthly mean shortwave flux under all-sky conditions, named "toa\_sw\_all\_mon", for the period July 2000–June 2020. The data can be ordered and freely obtained at [84].

### 2.1.3. GEBA & BSRN

GEBA is a database of ground-based measurements, located at the Institute for Climate and Atmospheric Sciences ETH Zürich (Zürich, Switzerland). It provides mean monthly values of 15 energy flux components (global, diffuse and direct shortwave radiation, surface albedo, longwave downward and upward radiation, etc.) measured from 2500 globally distributed stations, with 500,000 monthly values. Many stations provide measurements since the 1950s and some of them back to the 1930s. Their accuracy, in terms of relative random measurement error, has been estimated by [19] at 5% of the monthly means, and 2% of the yearly means. SSR monthly data, mostly measured by pyranometers, are collected from 1397 stations for the time period 1980–2017 [85,86]. The GEBA data are available at no cost for bona fide research after registration at [87].

The BSRN is a project of the Radiation Panel of the GEWEX under the World Climate Research Programme (WCRP). Its goal is to provide radiation measurements of high quality and high temporal resolution (one to three minutes) at sites (presently 73) located in various climate zones around the world since January 1992. These measurements are reported to the BSRN Archive at the Alfred Wegener Institute (AWI) in Bremerhaven, Germany. In this study SSR measurements taken from 73 BSRN stations for the time period 1992–2020 are utilized. The BSRN sites can measure the direct shortwave flux (measured with a pyrhelimeter) and the diffuse shortwave flux (measured with a shaded pyranometer), apart from the global shortwave flux (measured with a pyranometer). The quality of the BSRN solar and thermal radiation data is reported in [88]. Using single pyranometers in conjunction with the component sum method at BSRN sites [85], and considering long term averaging, an accuracy up to  $5 \text{ Wm}^{-2}$  ( $\sim 2\%$  for 24-h mean solar irradiance) has been estimated, meeting the BSRN specifications under optimal observing conditions. The mean monthly BSRN data used for the evaluation of MERRA-2 SSR and GDB are computed from daily data, which are in turn calculated from the instantaneous (minute level) data. Care is taken to ensure the representativeness and accuracy of the computed monthly mean BSRN data. To this aim, if more than 25% of the total instantaneous measurements during the daytime of one day are missing, the daily integrated SSR values are excluded. Then, in the next step of the computation of BSRN monthly SSR fluxes, if more than five daily SSR data are missing in one month, the monthly SSR data are excluded from the comparison. The BSRN data were freely downloaded via PANGAEA or ftp at [89]. The global distribution of the originally available GEBA and BSRN stations shown in Figure S1. The stations, especially the GEBA ones, cover almost the entire globe (continental areas) with a better or worse density, whereas there is a dense network of stations in Europe and Eastern Asia.

### 2.2. Methodology

The evaluation of MERRA-2 GDB is examined through comparisons against GEBA and BSRN measurements using monthly mean SSR fluxes and deseasonalized anomalies, which were computed by subtracting from each monthly SSR value the corresponding long-term (different for each station) averaged value. SSR anomalies were preferred to corresponding absolute fluxes in the computation of either the correlation coefficients or the trends of time series, since the use of deseasonalized anomalies minimizes the seasonal component of variability, which is assumed to be periodic with constant amplitudes and thus does not have much impact on the long-term variability [90]. On the other hand, the computation of other evaluation statistical metrics, such as the absolute and relative percent bias and root mean squared error (RMSE), were done using the absolute monthly SSR fluxes. Specific data availability criteria have been applied in the analysis in order to ensure the maximum possible robustness of the obtained results and conclusions. Thus, in the comparison between MERRA-2 and GEBA/BSRN SSR fluxes and anomalies, each year was required to have more than 10 months of measurements available, in order to exclude years with poor seasonal representativeness, which would degrade the comparison quality. The application of this criterion resulted in availability of 1099 GEBA and 70 BSRN stations (out of the originally available 1397 GEBA and 73 BSRN stations). These stations, shown in

Figure 1, still ensure a satisfactory geographical coverage of the world’s continental areas, of course more for GEBA than BSRN. The different steps of the applied methodology are outlined in Figure 2.

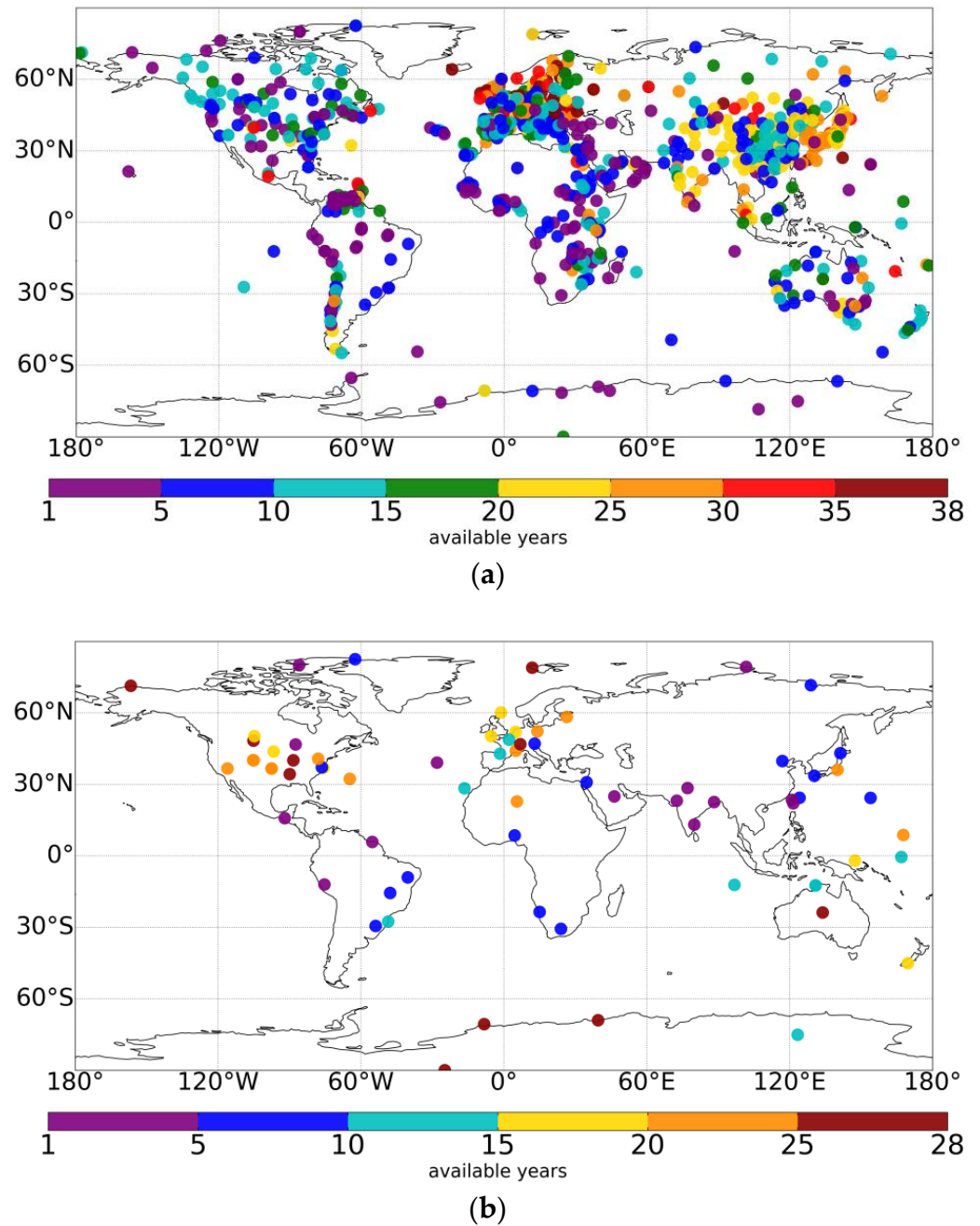


**Figure 1.** Global Distribution of: (a) Global Energy Balance Archive (GEBA) 1099 stations and (b) Baseline Surface Radiation Network (BSRN) 70 stations, whose surface solar radiation (SSR) data (availability in years indicated in the colorbar) have been used in this study.

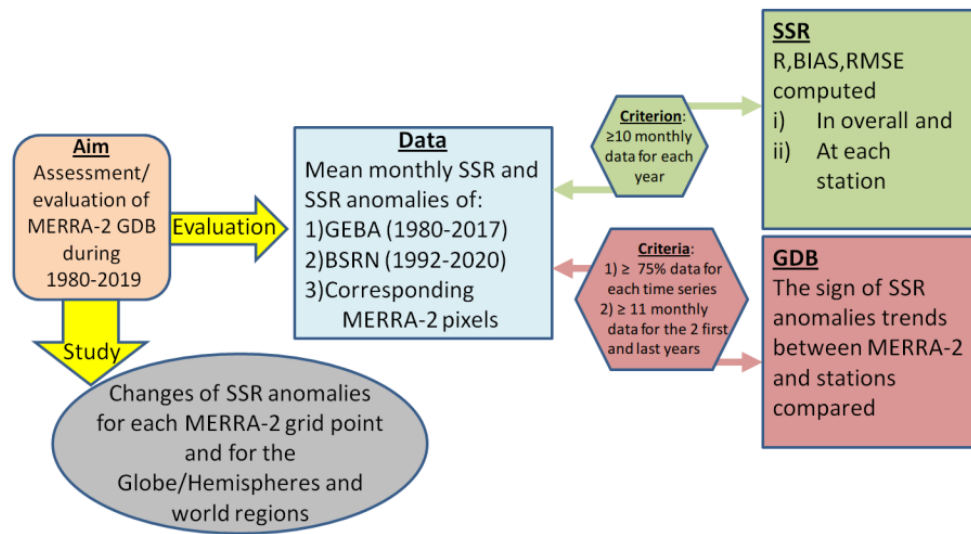


**Figure 2.** The steps of the applied methodology of assessment/evaluation of MERRA-2 GDB.

Four (4) statistical indices were used to quantify the degree of agreement/disagreement between the MERRA-2 and reference stations’ GDB: the Pearson’s correlation coefficient (R), the Root Mean Squared Error (RMSE) and percent relative RMSE (RRMSE), the bias and relative bias; whose equations are:

$$R = \frac{\sum_{i=1}^n (M_i - M)(G_i - G)}{\sqrt{\sum_{i=1}^n (M_i - M)^2} \sqrt{\sum_{i=1}^n (G_i - G)^2}} \tag{1}$$

$$RMSE = \sqrt{\frac{1}{n} \sum_{i=1}^n (M_i - G_i)^2} \tag{2}$$

$$RRMSE = \frac{\sqrt{\frac{1}{n} \sum_{i=1}^n (M_i - G_i)^2}}{G} 100\% \tag{3}$$

$$BIAS = M - G \tag{4}$$

$$BIAS(\%) = \frac{M - G}{G} 100\% \tag{5}$$

where  $n$  is the number of monthly data,  $M_i$  and  $G_i$  are the monthly (for the  $-i$  month) values of MERRA-2 and ground-based station, respectively, and  $M$  and  $G$  are the mean values of MERRA-2 and ground-based stations. The R (Equation (1)) value measures how strongly the two variables correlate (covariate), whereas RMSE (Equation (2)) measures the average magnitude of the error, i.e., the difference between the Reanalysis and ground station. Since the errors are squared before being averaged, the RMSE gives a relatively high weight to large errors, thus it is most useful when large errors are particularly undesirable. The normalized RMSE (Equation (3)) is also computed. BIAS quantifies the difference between the mean value of predictions and the mean value of observations, as shown in Equation (4). Emphasis, however, is also placed on relative bias, which better represents the difference (Equation (5)). In order to evaluate the GDB of MERRA-2, a linear regression was applied to the time series of deseasonalized monthly anomalies, and the slopes were computed either for each station or the corresponding MERRA-2 pixels, where the stations are located. To achieve greater confidence in the estimated slopes, we used a criterion of sufficient data availability, according to which: (a) each time series should have a availability of monthly values of more than 75% of the total period of each network and (b) the first two and last two years should have more than 10 months available. This was decided because of the sensitivity of linear trends to the initial and latest parts of time series (as done in [91]). These



criteria were satisfied for 232 GEBA and 22 BSRN stations (shown in the graphs presented in the next section, i.e., results). The slope values were calculated using the more robust, nonparametric Theil-Sen's slope estimator [92,93], which is the median of all possible linear slopes. The SSR changes ( $\Delta$ SSR) were computed by multiplying the computed slopes, which measure the changes per month, by the temporal duration (in number of months) for each time series. Along with the slopes, the statistically significant slopes at 95% confidence level were calculated using the non-parametric Mann-Kendall Test [94,95], which is used to determine whether a time series has a monotonic upward or downward trend or not. Then, the sign of the slope values for each station was compared with the sign of the slope of the corresponding MERRA-2 pixel (including the station). Same signs of slopes of the MERRA-2 and stations' time series of SSR anomalies indicate a qualitative agreement of  $\Delta$ SSR (or GDB) between MERRA-2 Reanalysis and GEBA/BSRN stations, for a specific pixel, whereas opposite trends indicate a disagreement. This evaluation is useful since it quantifies the degree to which the MERRA-2 based GDB agrees, in sign and magnitude, with the reference ground-based stations, providing confidence about the MERRA-2 GDB.

### 3. Results

#### 3.1. Evaluation of MERRA-2 SSR

First, a comprehensive evaluation of MERRA-2 SSR, which is prerequisite for the evaluation of MERRA-2 GDB, is attempted in this section. The evaluation is made either on a total, i.e., all stations (Section 3.1.1) or on an individual station (Section 3.1.2) basis. It should be noted that apart from absolute SSR fluxes, SSR deseasonalized anomalies are also used in the correlations between the Reanalysis and stations fluxes in order to remove the significant contribution of the seasonal cycle of solar radiation.

##### 3.1.1. All Stations

The metrics of the overall comparison of MERRA-2 SSR fluxes and anomalies with the corresponding measurement-based fluxes and anomalies from 1099 GEBA and 70 BSRN stations are given in Table 1, whereas the associated scatterplot comparisons are shown in Figure 3. It seems that MERRA-2 SSR anomalies correlate satisfactorily with the station measurements (Table 1), yielding R values equal to 0.61 and 0.62 for GEBA and BSRN, respectively (the corresponding R values using SSR fluxes are, as expected, much higher, equal to 0.95 and 0.97). Overall, MERRA-2 overestimates SSR with respect to GEBA and BSRN, having positive mean absolute biases equal to 24.25 and 10.31  $\text{Wm}^{-2}$ , respectively, corresponding to respective relative biases equal to 15.3% and 5.9%. It should be noted that as reported in the literature [96] the Chinese stations from GEBA may not be so representative for  $0.5^\circ$  grid boxes due to strong urbanization effects. Thus, the evaluation of MERRA-2 SSR against GEBA stations was repeated excluding the Chinese stations, which, indeed, led to a reduction of the MERRA overestimation by 13.6%. The MERRA overestimation with respect to GEBA/BSRN may lead to the conclusion that the atmosphere of MERRA-2 is more transparent, which is in agreement with other studies [44], possibly caused by an underestimation either of cloud cover or aerosol loadings, i.e., aerosol optical depth (AOD), which are the main drivers of GDB [12,22]. Apart from the mean bias error, another significant statistical metric, showing how far from the regression line the data points are, is the RMSE, which is equal to 36.07  $\text{Wm}^{-2}$  for GEBA and 26.12  $\text{Wm}^{-2}$  for BSRN (corresponding to 22.8% and 15.1% of the station networks' mean values). These results, along with the obtained biases, show that MERRA-2 deviates less from the values of BSRN and a little more than from values of GEBA. A slightly better fitting of the applied linear regression line is also obtained for BSRN than GEBA, as indicated by the respective slope values of 0.99 and 1.04 (the corresponding values for SSR anomalies are equal to 0.50 and 0.47). Note that in a similar evaluation of MERRA SSR, but over the significantly shorter period 2001–2009, [39] estimated R values equal to 0.96 (0.82) for GEBA stations and 0.98 (0.92) for BSRN (numbers in parentheses give the R values computed using deseasonalized anomalies), i.e., again higher for BSRN than GEBA. They also reported a better performance

of MERRA against BSRN than GEBA stations in terms of RMSE values (equal to 23.99 Wm<sup>-2</sup> for BSRN and 32.27 Wm<sup>-2</sup> for GEBA) as well as for bias (13.80 Wm<sup>-2</sup> for BSRN and 22.17 Wm<sup>-2</sup> for GEBA). In another evaluation of MERRA-2 SSR against GEBA and China Meteorological Administration (CMA) stations, [38], computed R values equal to 0.94 and 0.95 for the 1990–1999 and 2000–2009 periods, respectively. Our computed statistical metrics are in general agreement with the findings from the few existing evaluations of MERRA-2 SSR but provide more confidence about the obtained conclusions regarding the performance of the Reanalysis against the two reference ground station networks, since they refer to a much longer time period (up to about 40 years for GEBA and 30 years for BSRN). Moreover, the present study more thoroughly and appropriately evaluates the covariation of MERRA-2 SSR with stations, since it also estimates the correlation coefficients using SSR deseasonalized anomalies, which is more meaningful and appropriate.

**Table 1.** Comparison between MERRA-2 and GEBA/BSRN SSR on an annual and seasonal basis, along with the computed main statistical parameters (number of matched data pairs, N, slope value of applied linear regression fit, absolute and percent relative biases of MERRA-2 relative to the mean GEBA/BSRN values, root mean squared error, RMSE, percent relative RMSE (RRMSE) with respect to the mean GEBA/BSRN values, correlation coefficient, R, the mean GEBA and BSRN values and the number of available stations, id, whose SSR measurements are used in the comparison). In addition, the R and slope values computed using deseasonalized SSR anomalies are given in parentheses.

MERRA-2-GEBA	Annual	DJF	MAM	JJA	SON
N	197,302	49,067	49,501	49,357	49,377
slope	1.04 (0.47)	1.05 (0.46)	0.92 (0.51)	0.85 (0.44)	1.02 (0.46)
BIAS	24.25	15.49	26.37	33.52	21.58
BIAS(%)	15.3	15.5	14.1	15.6	16.5
RMSE	36.07	27.62	38.65	44.58	30.95
RRMSE(%)	22.8	27.7	20.7	20.7	23.7
R	0.95 (0.61)	0.96 (0.56)	0.88 (0.65)	0.85 (0.60)	0.95 (0.59)
mean_GEBA	158.36	99.78	186.89	215.50	130.85
mean_MERRA-2	182.61	115.27	213.26	249.03	152.42
id	1099	1099	1099	1099	1099
MERRA-2-BSRN	Annual	DJF	MAM	JJA	SON
N	11,259	2807	2826	2800	2826
slope	0.99 (0.50)	0.96 (0.51)	1.00 (0.50)	0.99 (0.46)	0.98 (0.53)
BIAS	10.31	5.84	10.46	14.45	10.51
BIAS(%)	5.9	4.1	5.5	6.8	6.8
RMSE	26.12	22.32	27.15	29.88	24.51
RRMSE(%)	15.1	15.9	14.4	14.1	15.9
R	0.97 (0.62)	0.98 (0.61)	0.95 (0.63)	0.96 (0.60)	0.97 (0.63)
mean_BSRN	173.57	139.60	188.90	212.10	153.82
mean_MERRA-2	183.89	145.44	199.4	226.5	164.33
id	70	70	70	70	70

Apart from assessing the performance of MERRA-2 SSR on an annual basis, this has also been done on a seasonal basis, since this may help to identify possible source of errors. It should be noted that, due to the substantial seasonal variation of SSR fluxes, not only the absolute, but also the relative biases were computed. According to Table 1, R and relative percent bias do not show significant seasonal changes, apart from slightly (by up to 0.1) lower R values in boreal spring and summer, especially for GEBA, and better in winter and autumn. This is not valid for R computed with deseasonalized SSR anomalies, which is best in spring (and autumn for BSRN). On the other hand, BIAS and RMSE have a remarkable seasonal range, up to about 18/8.5 W/m<sup>2</sup> for bias and GEBA/BSRN, respectively, and up to about 17/8 W/m<sup>2</sup> for RMSE and GEBA/BSRN, respectively, being largest in summer due to the largest absolute amounts of SSR. Similar findings for RMSE and bias were found by [38], who used GEBA and CMA station SSR measurements, and by [39], who used GEBA and BSRN station measurements, but for shorter time periods. Besides, the relative RMSE doesn't exhibit significant seasonal changes (they are less than 7/1.9 W/m<sup>2</sup> for GEBA/BSRN respectively). The obtained metrics are generally better for the comparison with BSRN than GEBA station measurements, which is encouraging, given the higher quality of this network [88]. In order to more effectively assess the seasonal performance of MERRA-2 SSR, and given the systematic 6-month shift of extreme seasons between the two hemispheres, the seasonal variation of main statistical metrics, namely R, RMSE (in absolute

and % terms) and bias (in absolute and % terms) were also computed separately for the two hemispheres and they are given in Figure 4. The results of this figure were obtained using SSR fluxes except for R, which is computed using deseasonalized SSR anomalies (the corresponding R using absolute SSR fluxes is given in Figure S3). As shown in Figure 4, there are high bias and RMSE values in summer in both hemispheres. Nevertheless, it must be taken into account that these values correspond to the highest summer values of SSR. In contrast, the highest relative bias (17.9%) and RRMSE (30.9%) values are in winter in both hemispheres (Figure 4c,e). Similarly, the R values computed using deseasonalized SSR anomalies are lowest in winter (0.52). These results indicate that the MERRA-2 SSR perform worst in the cold period of the year. The different performance of the reanalysis SSR products with seasons may be due to the seasonally varying deficiencies in the reanalysis cloud coverage, aerosol optical depth or water vapor [39,47].

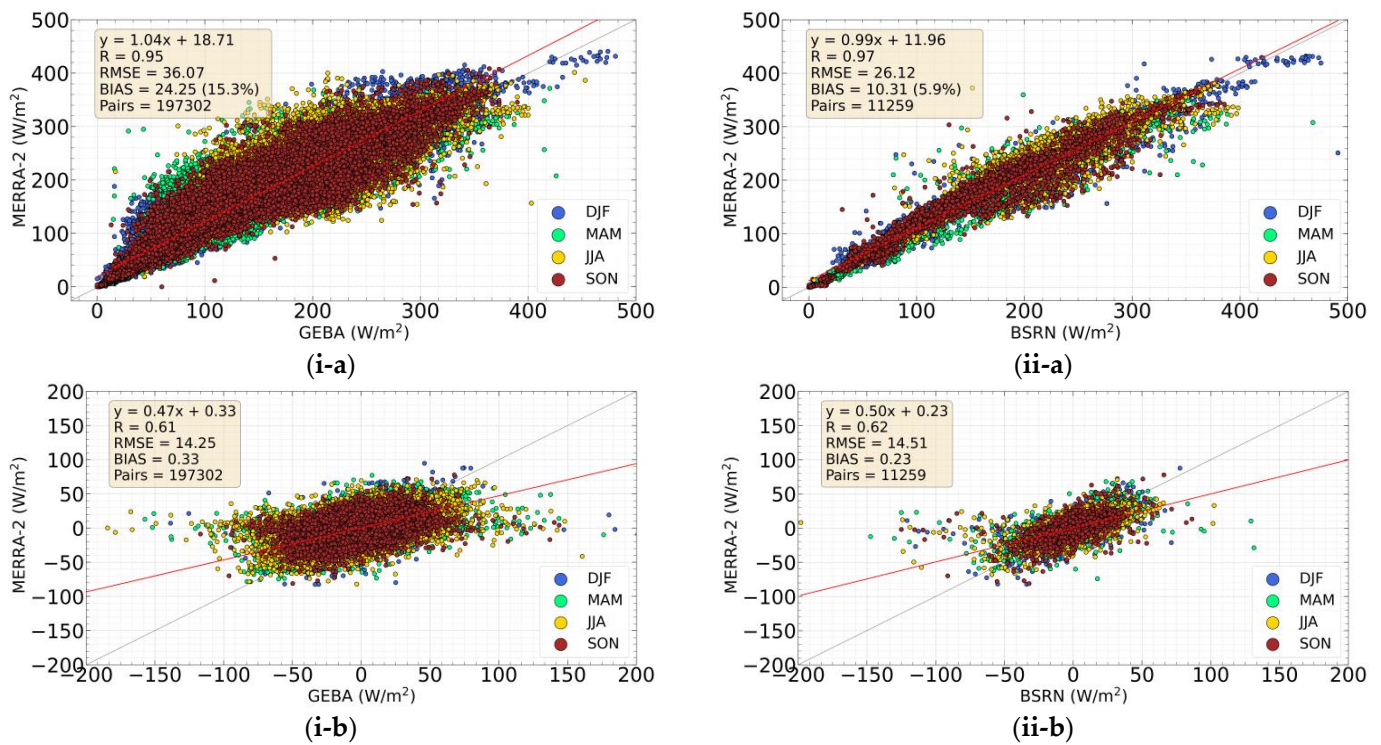


**Figure 3.** Scatterplot comparison between MERRA-2 Reanalysis and GEBA (i-a), and BSRN (ii-a) SSR fluxes and between MERRA-2 and GEBA (i-b) and BSRN (ii-b) deseasonalized SSR anomalies. The linear regression fit, and the associated statistical metrics, namely the equation of the applied linear fitting, the correlation coefficient (R), the root-mean squared error (RMSE), the bias and the total number of matched data pairs, are also shown. The comparison is shown separately for each season (December–February, March–May, June–August and September–November) in different colors (the respective main statistical parameters are given in Table 1).

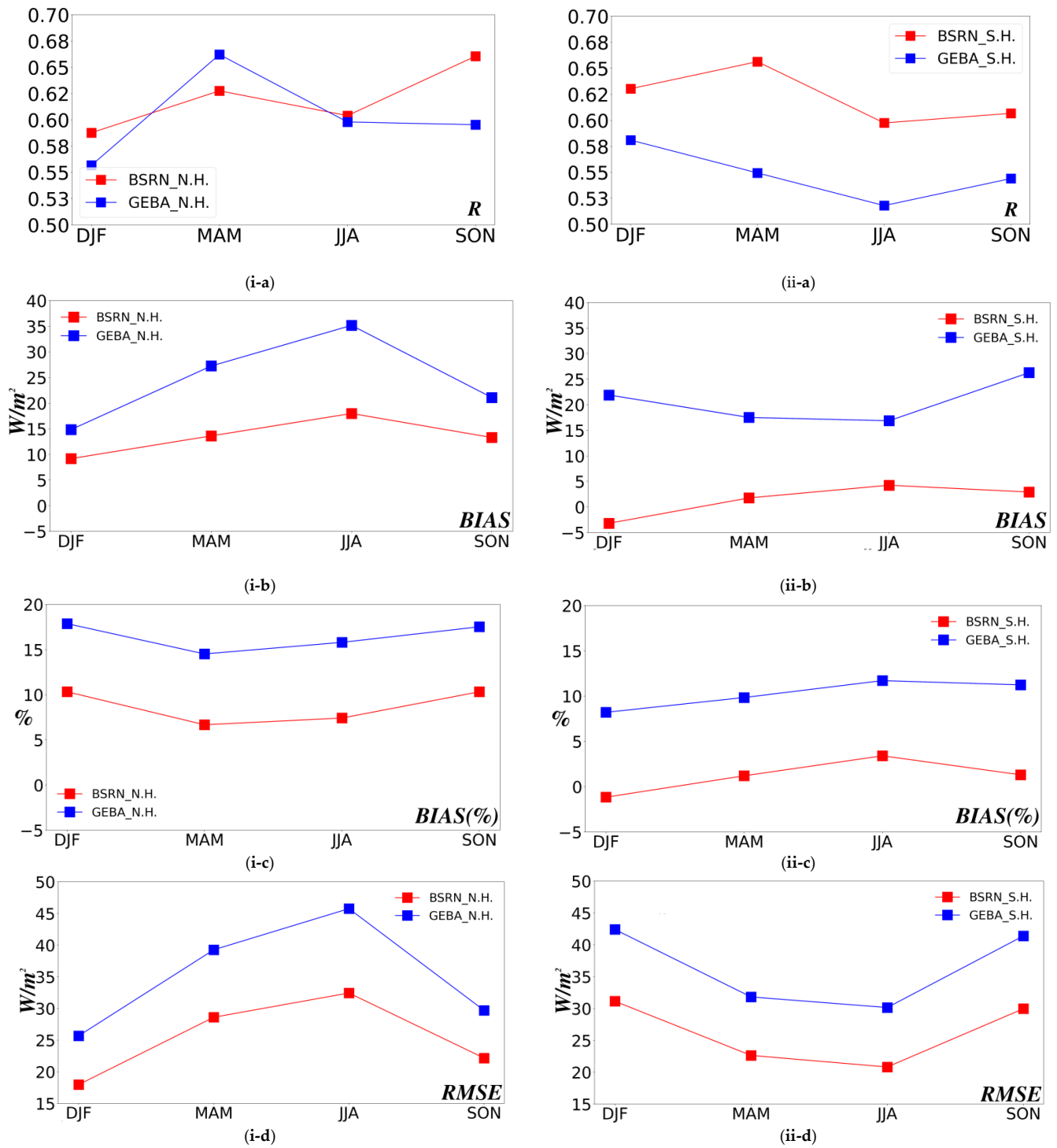
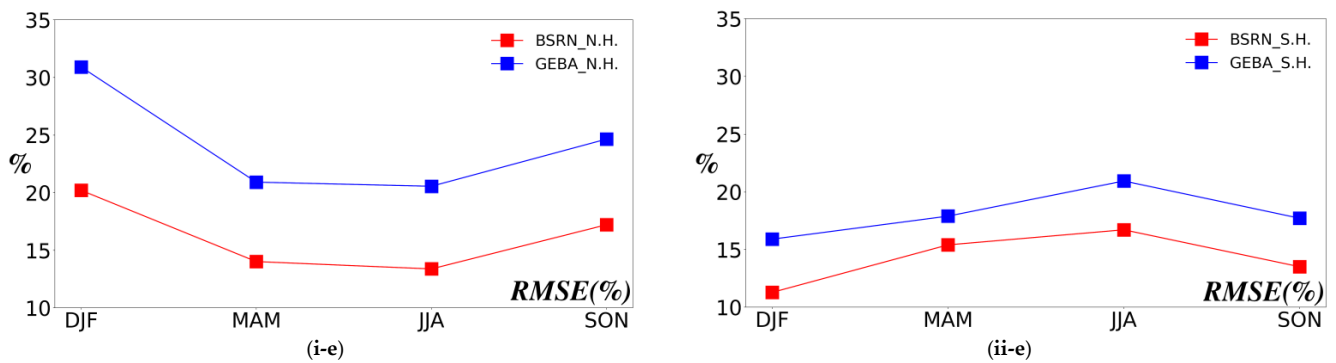


Figure 4. Cont.





**Figure 4.** Seasonal variation of hemispherical averages of correlation coefficient  $R$  (i,ii-a), bias in  $W/m^2$  (i,ii-b), percent relative bias in % (i,ii-c), root mean squared error (RMSE in  $W/m^2$ ) (i,ii-d) and percent relative RMSE in % (i,ii-e) between MERRA-2 and GEBA (blue) and BSRN (red) stations, computed using SSR fluxes (except for  $R$  that is computed using deseasonalized SSR anomalies) for the North Hemisphere ((i)-left column) and South Hemisphere ((ii)-right column).

### 3.1.2. At Station Level

In the context of evaluating the MERRA-2 SSR, it is necessary to examine and compare the fluxes on an individual station basis to identify possible dependencies on latitude or regional patterns. The spatial distribution of correlation coefficient ( $R$ ) computed using deseasonalized SSR anomalies, RMSE, RRMSE, bias and relative bias, computed using SSR fluxes, between MERRA-2 and GEBA/BSRN stations are shown in Figure 5. The average value of  $R$  for all GEBA stations is 0.54, ranging from  $-0.25$  to  $0.92$ , while for BSRN stations it is 0.54 and ranges from  $0.15$  to  $0.89$ . For more than 75% of GEBA/BSRN stations the  $R$  values are larger than  $0.49/0.51$  (Figure S5). Satisfactory  $R$  values (orange and reddish colors) appear over Europe, East Asia, North America and Australia, along with mixed patterns over Africa and South America. On the contrary, worse  $R$  values exist mostly over the tropical and sub-tropical regions of the globe, including Africa, Southern America, India and Indonesia. A similar behavior is found for  $R$  computed with SSR fluxes (Figure S4). Given that clouds are one of the main factors driving the SSR [10], and that in the tropics there is constantly large cloud cover, it can be assumed that the small correlation of MERRA-2 in these areas may be due to uncertainties in MERRA-2 cloud cover and optical properties, as also suggested by other studies [39,47]. This is not unexpected since it has been shown that clouds are associated with the greatest uncertainty in climate modeling (e.g., [97,98]). Relatively weak correlation is also found in relatively cloud-free areas like the Middle East and Egypt possibly due to uncertainties in MERRA-2 aerosols. Weak correlation is found in polar regions as well, where the discrepancies could be due to problems with clouds, but also with snow and ice cover [44,99]. Concerning the  $R$  computed using absolute SSR fluxes, it can be noted (Figure S4) that the  $R$  values are lower in southern than in northern China. Such a pattern has been also reported in other studies, and has been attributed to the heavy air pollution, as well as to uncertainties in clouds, aerosols and their interaction [39]. Nevertheless, this pattern is not apparent in the results of  $R$  computed using SSR anomalies, where weak correlation coefficients are scattered all around China, revealing that correlating reanalysis and station SSR fluxes and SSR anomalies is not driven by the same factors.

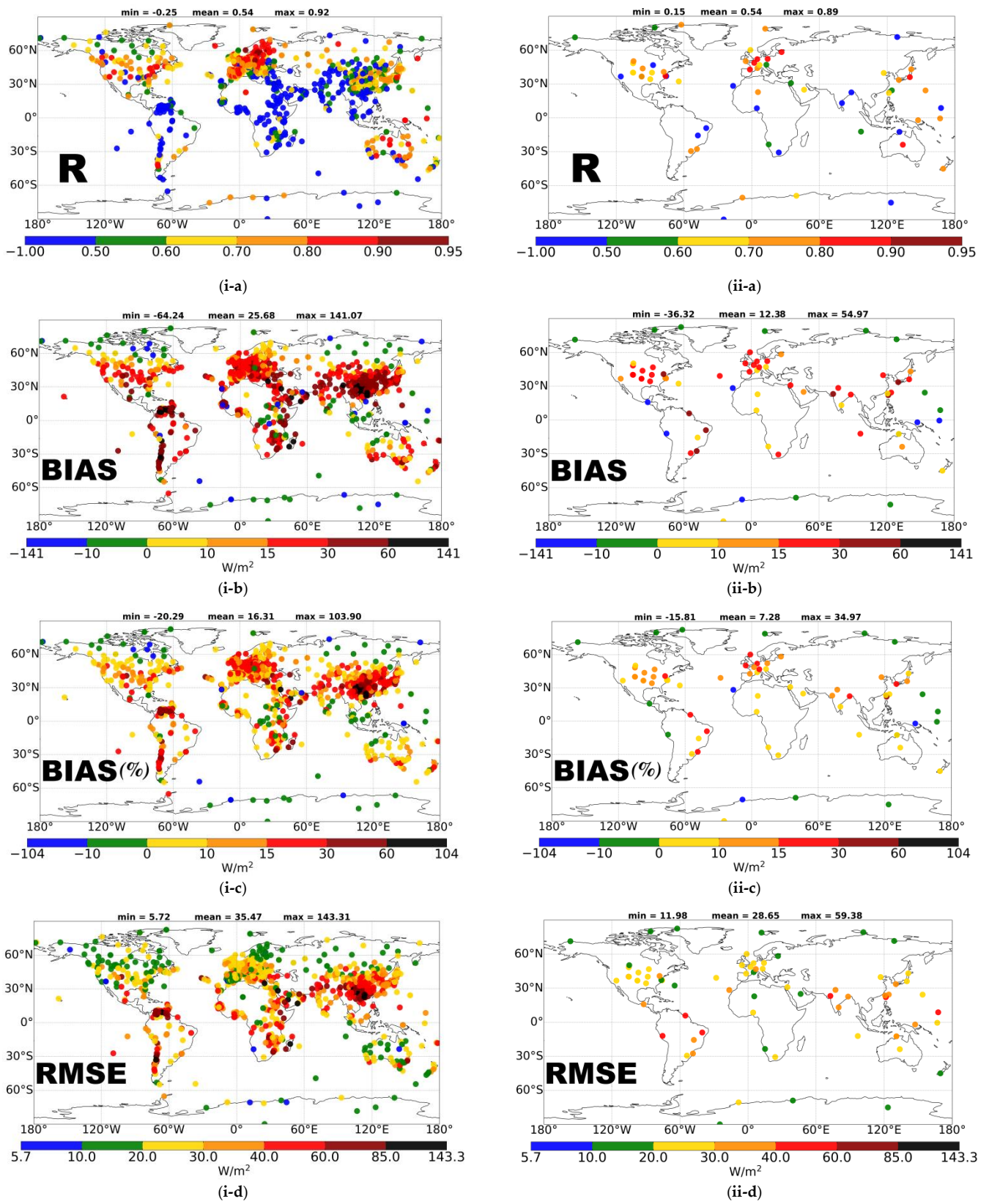
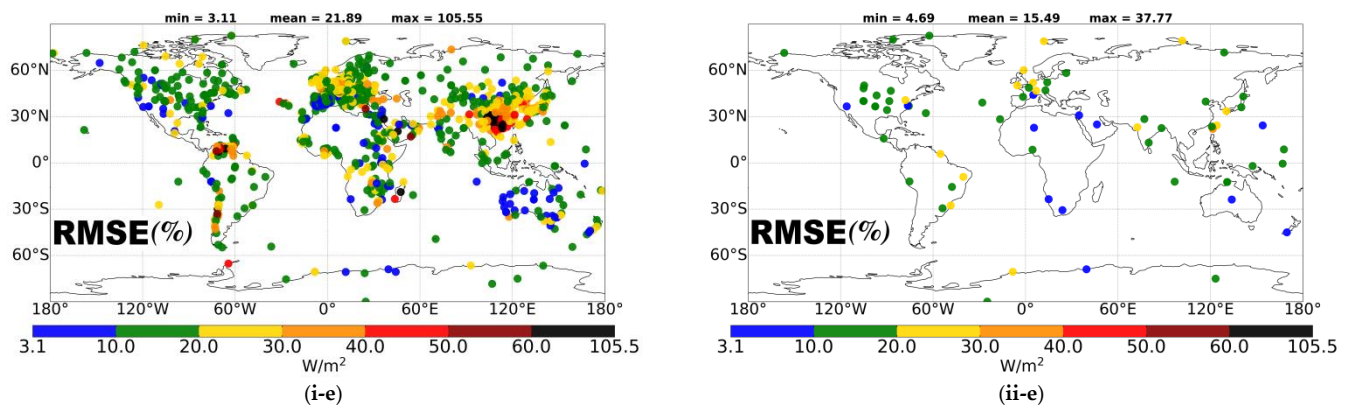


Figure 5. Cont.



**Figure 5.** Global distribution of correlation coefficient (i,ii-a), bias (i,ii-b) and relative percent bias (i,ii-c) root mean squared error (i,ii-d), relative root mean squared error (i,ii-e), computed for the comparison between MERRA-2 and each GEBA ((i), left column) and BSRN ((ii), right column) station SSR fluxes, except for R that is computed using deseasonalized SSR anomalies.

Large RMSE values are computed over tropical and sub-tropical regions, confirming the difficulties of MERRA-2 to appropriately reproduce SSR there. The average RMSE for all GEBA stations is  $35.47 \text{ W/m}^2$ , with values ranging from  $5.72$  to  $143.31 \text{ W/m}^2$  and with 75% of GEBA stations having RMSE less than  $40.3 \text{ W/m}^2$ . Respectively, the average RMSE for all BSRN stations is  $28.65 \text{ W/m}^2$ , still lower than the corresponding value for GEBA, ranging from  $11.98$  to  $59.38 \text{ W/m}^2$  and with 75% of BSRN stations having RMSE less than  $31.9 \text{ W/m}^2$  (Figure S5). Similar geographical patterns appear for the relative RMSE, for which 75% of GEBA/BSRN stations have values smaller than 26.1%/20.3% and with high values found especially over Southern China, North Europe and some tropical and subtropical regions.

The obtained results for the absolute and relative bias show that MERRA-2 generally overestimates SSR (both absolute fluxes and their anomalies) with respect to GEBA, underestimating it (green and blue colors in Figure 5) over some tropical, subtropical, polar and subpolar regions. Specifically, concerning SSR fluxes, MERRA-2 overestimates SSR in 998 stations and underestimates it in only 101 stations, resulting in an overall overestimation equal to  $24.25 \text{ W/m}^2$ . On the other hand, concerning the comparison against the much fewer (70) BSRN stations, MERRA-2 shows an overall overestimation of SSR fluxes by  $10.31 \text{ W/m}^2$  (53 out of 70 overestimate). The average value of the absolute and relative % bias for all GEBA stations is  $25.68 \text{ W/m}^2$  and 16.3%, respectively, with values ranging from  $-64.24$  to  $141.07 \text{ W/m}^2$  and from  $-20.3$  to  $103.9\%$ , respectively. 75% of the GEBA stations have absolute and relative % bias values less than  $33.21 \text{ W/m}^2/21.9\%$ , respectively (Figure S5). Smaller biases are found against BSRN stations, namely an average absolute and relative % bias equal to  $12.38 \text{ W/m}^2$  and 7.3%, respectively, with relative % and absolute bias values ranging from  $-15.8$  to  $35\%$ , and from  $-36.32$  to  $54.97 \text{ W/m}^2$ , respectively, and with 75% of the stations having relative % and absolute bias less than 13.7%/20.83  $\text{W/m}^2$ , respectively.

Focusing on China, where many stations and more similar studies to the present one exist, our results are in line with the study of [65], who evaluated both MERRA-2 and MERRA SSR fluxes against 2400 CMA stations from 1980 to 2014 and reported that MERRA-2 has a high mean bias over China, which is greater in its southern part, due to its incorrect assessment of cloud fraction and aerosol loadings. Moreover, previous studies [37,47,96,100,101] have reported that aerosols might be another important source of the large positive biases in China, where the rapid economic development produced large amounts of pollution. The results obtained by ([39], and references therein) further proved that the biases in the MERRA, Era-interim, JRA-55, NCEP-NCAR, NCEP/DOE and CFSR reanalysis cloud fraction result in SSR biases, and that both clouds and aerosol representation schemes should be improved in the reanalysis estimates.

### 3.2. MERRA-2 GDB (SSR Trends) and Its Evaluation

After the evaluation of MERRA-2 SSR fluxes, which proved a relatively good performance, a thorough evaluation of their inter-decadal (1980–2017) changes, namely of the MERRA-2 GDB, is presented here. It should be noted that such an evaluation of MERRA-2 GDB has not been made to date, and it is worth doing given the long temporal coverage of this reanalysis SSR dataset. The evaluation is made either on a total (all stations) or on an individual station basis (Section 3.2.1). After the GDB evaluation, the gridded MERRA-2 GDB all over the globe, as well as on a global and regional mean basis is assessed and discussed in Section 3.2.2.

#### 3.2.1. Evaluation of MERRA-2 GDB (SSR Trends)

The evaluation of MERRA-2 GDB was made against corresponding GDB estimates from the reference GEBA and BSRN station networks. More specifically, comparisons were performed between GDB ( $\Delta$ SSR) of the MERRA-2 pixels including the GEBA or BSRN stations. The two sets of GDB, i.e., the MERRA-2 and stations ones, were computed by applying linear regression to the corresponding time series of monthly mean deseasonalized SSR anomalies and subsequently computing the slope values. This analysis was made for 232 GEBA and 22 BSRN stations, the number of stations being determined based on the applied strict availability criteria reported in Section 2.2 ensuring a sufficiently strong reliability of the findings. It should be noted here that the time period is not the same for all stations, being determined by the original temporal coverage of every station's measurements and the applied availability criteria, and ranges from 27 to 38 years for GEBA stations and 20 to 28 years for BSRN stations (as shown in Figure S2, Supplementary Materials). The length of MERRA-2 records adjusted accordingly to each station's time period.

#### All Stations

The scatterplot comparison between the SSR (anomaly) trends ( $W/m^2$ ) of the MERRA-2 and GEBA/BSRN stations is shown in Figure 6. On average, the MERRA-2 SSR trends correlate weakly with the corresponding ones of GEBA/BSRN stations, yielding average R values equal to 0.32/0.30. The computed RMSE values are equal to 12.97/8.37  $W/m^2$  for GEBA/BSRN, while the computed biases (MERRA-2 GDB—stations GDB), equal to  $-3.99/-3.57 W/m^2$  for GEBA/BSRN, show an overall underestimation of MERRA-2. The number of matched data pairs of Figure 6 lying in the first and third quartiles (positive-positive and negative-negative, i.e., with both reanalysis and stations brightening and dimming, respectively) are 117 and 29 for MERRA-GEBA (corresponding to 50 and 12.5% of the total number of points for the MERRA-GEBA scatterplot) and 6 and 5 for MERRA-BSRN (corresponding 27/23% of the total number of points for the MERRA-BSRN scatterplot). These results indicate that MERRA-2 Reanalysis yields the same sign of GDB in 63 and 50% of GEBA and BSRN stations.

In order to also examine the similarity/dissimilarity between the inter-annual variation of MERRA-2 and GEBA/BSRN stations' SSR anomalies, the averaged SSR anomalies of all stations and the corresponding MERRA-2 pixels over the total period for each network, i.e., 1980–2017 for GEBA and 1992–2020 for BSRN, were computed and are given in Figure 7. The number of stations that were available in every month along with the 12-month moving averages is also shown. The overall correlation coefficient between MERRA-2 and GEBA is satisfactory (R equal to 0.8), while MERRA-2 shows systematically larger/smaller positive SSR anomalies than GEBA before/after the year 2000, leading to an average bias (MERRA-2—stations) equal to 1.25 and  $-1.93 W/m^2$  before and after 2000 (Figure 7a). Based on GEBA stations, a statistically significant brightening, i.e., positive  $\Delta$ (SSR), equal to  $3.96 W/m^2$  is found, versus a smaller ( $\Delta$ (SSR) =  $0.32 W/m^2$ ) and not statistically significant brightening according to MERRA-2. About similar conclusions are drawn from the corresponding comparison between MERRA-2 and BSRN (Figure 7b). The two time-series of SSR anomalies over the period 1992–2020 correlate well (R equal to



0.7), with positive ( $2.4 \text{ W/m}^2$ )/negative ( $-0.18 \text{ W/m}^2$ ) biases before/after 2000. Based on BSRN stations, a not statistically significant brightening, i.e., positive  $\Delta(\text{SSR})$ , equal to  $1.59 \text{ W/m}^2$  is found, versus a statistically significant dimming ( $\Delta(\text{SSR}) = -2.04 \text{ W/m}^2$ ) according to MERRA-2.

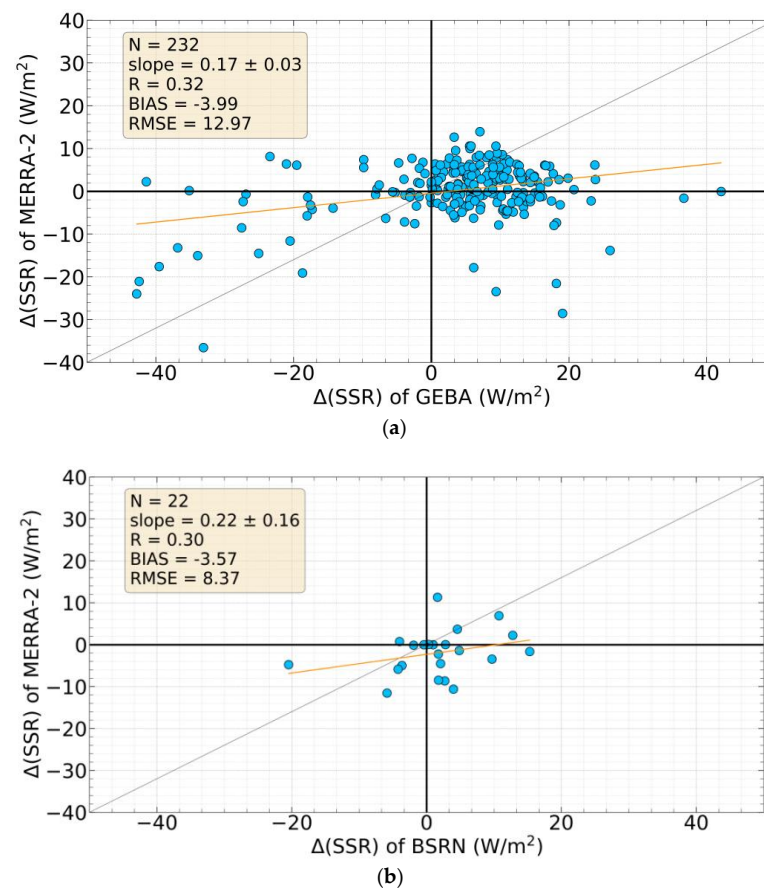
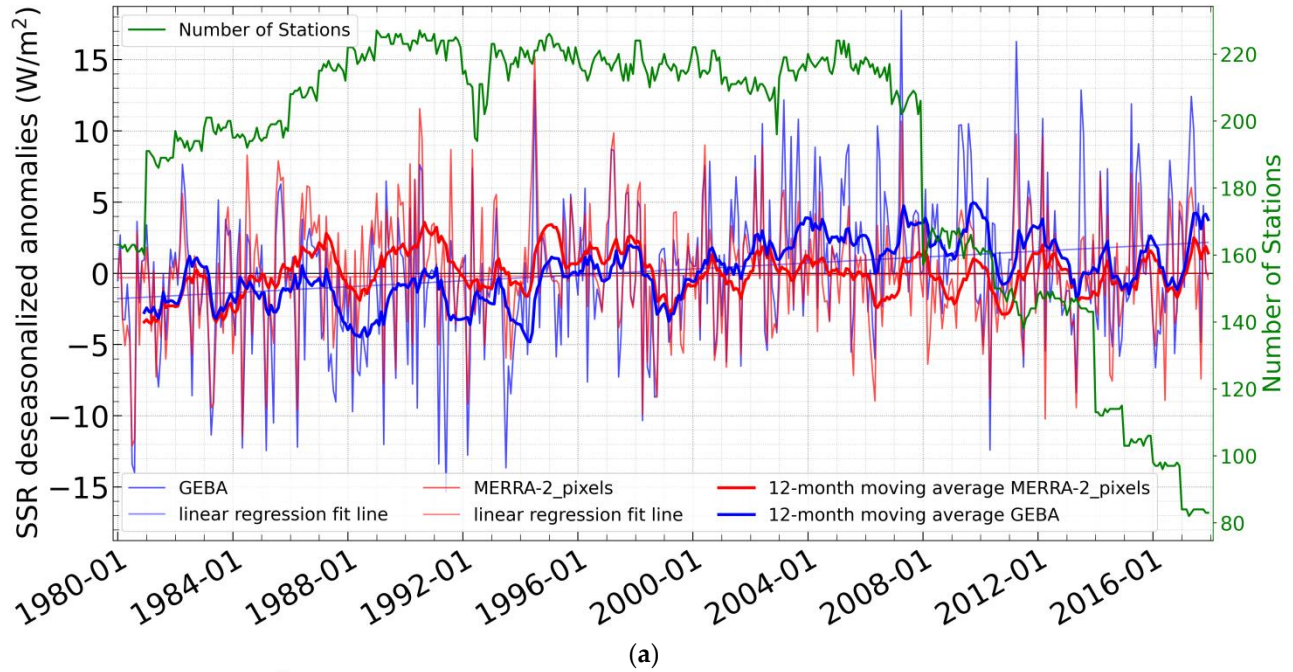


**Figure 6.** Scatterplot comparison between MERRA-2 and GEBA (a), and MERRA-2 and BSRN (b)  $\Delta(\text{SSR})$  or GDB (in  $\text{W/m}^2$ ). The linear regression fit, and the associated statistical metrics, namely the slope, the slope error, the correlation coefficient (R), the root-mean squared error (RMSE), the bias (MERRA-2 minus stations) and the total number of matched data pairs, are also shown.

#### At Station Level

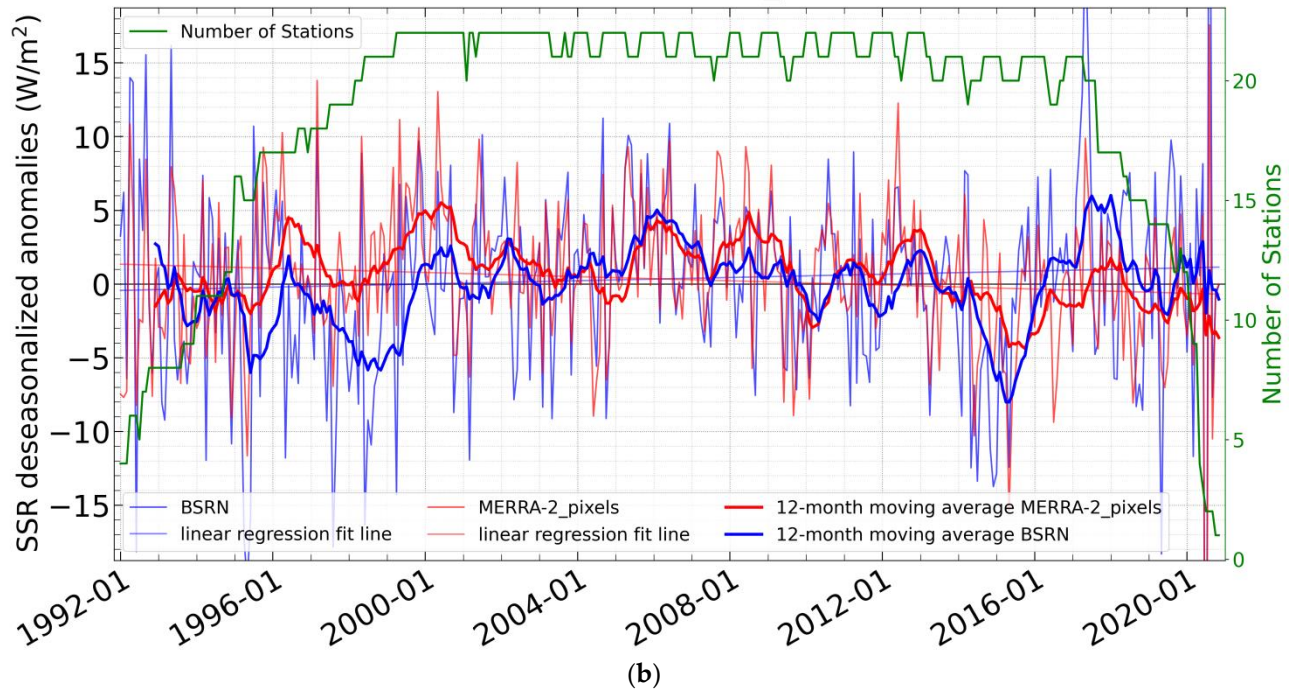
The GDB ( $\Delta(\text{SSR})$ ) for the GEBA/BSRN stations (the time period is different for each station) and the MERRA-2 pixels containing these stations are shown in Figure 8. These results enable the assessment of the GDB derived from stations and reanalysis, as well as the comparison between them. Apart from the computed trends, their statistical significance at the 95% level estimated applying the non-parametric Mann-Kendall test, is also presented in the Figure 8. The stations GDB results reveal many positive and statistically significant trends over Europe and East Asia, opposite to negative statistically significant trends over India. For GEBA stations, the positive trends vary from  $0.24$  to  $42.09 \text{ W/m}^2$ , and the negative trends from  $-0.28$  to  $-42.79 \text{ W/m}^2$ , whereas the corresponding ranges for BSRN stations are  $0.31$ – $15.3$  and  $-(0.41$ – $20.46) \text{ W/m}^2$ . It should be noted that independently of their sign, overall, statistically significant trends are found for 167 out of the 232 (i.e., for 72%) GEBA stations and for 103 out of the 232 (i.e., for 44.4%) of the corresponding MERRA-2 pixels. Respectively, statistically significant are the trends for 10 out of the 22 (45.4%) BSRN stations and for 9 out of the 22 (40.9%) corresponding MERRA-2 pixels. All examined 232 GEBA stations, indicate an average brightening of  $3.95 \text{ W/m}^2$ , while the BSRN stations indicate a somewhat weaker brightening of  $1.83 \text{ W/m}^2$ .

$\Delta(\text{SSR}) \pm \text{s.e. (W/m}^2\text{)}$ : GEBA =  $3.96 \pm 0.79$ , MERRA-2\_pixels =  $0.32 \pm 0.66$ , R = 0.80



(a)

$\Delta(\text{SSR}) \pm \text{s.e. (W/m}^2\text{)}$ : BSRN =  $1.59 \pm 1.35$ , MERRA-2\_pixels =  $-2.04 \pm 0.97$ , R = 0.70



(b)

**Figure 7.** Time series of averaged SSR anomalies for GEBA stations ((a), blue curve) and BSRN stations ((b), blue curve) along with those for the corresponding MERRA-2 pixels (red curves). The number of available stations for each month is also shown in green color. 12-month moving averages for each time series are also shown in same colors. The computed  $\Delta(\text{SSR})$  and the associated standard deviation along with the correlation coefficient (R) between the two sets of time series (1980–2017 for GEBA and 1992–2020 for BSRN) are given at the top of figure.

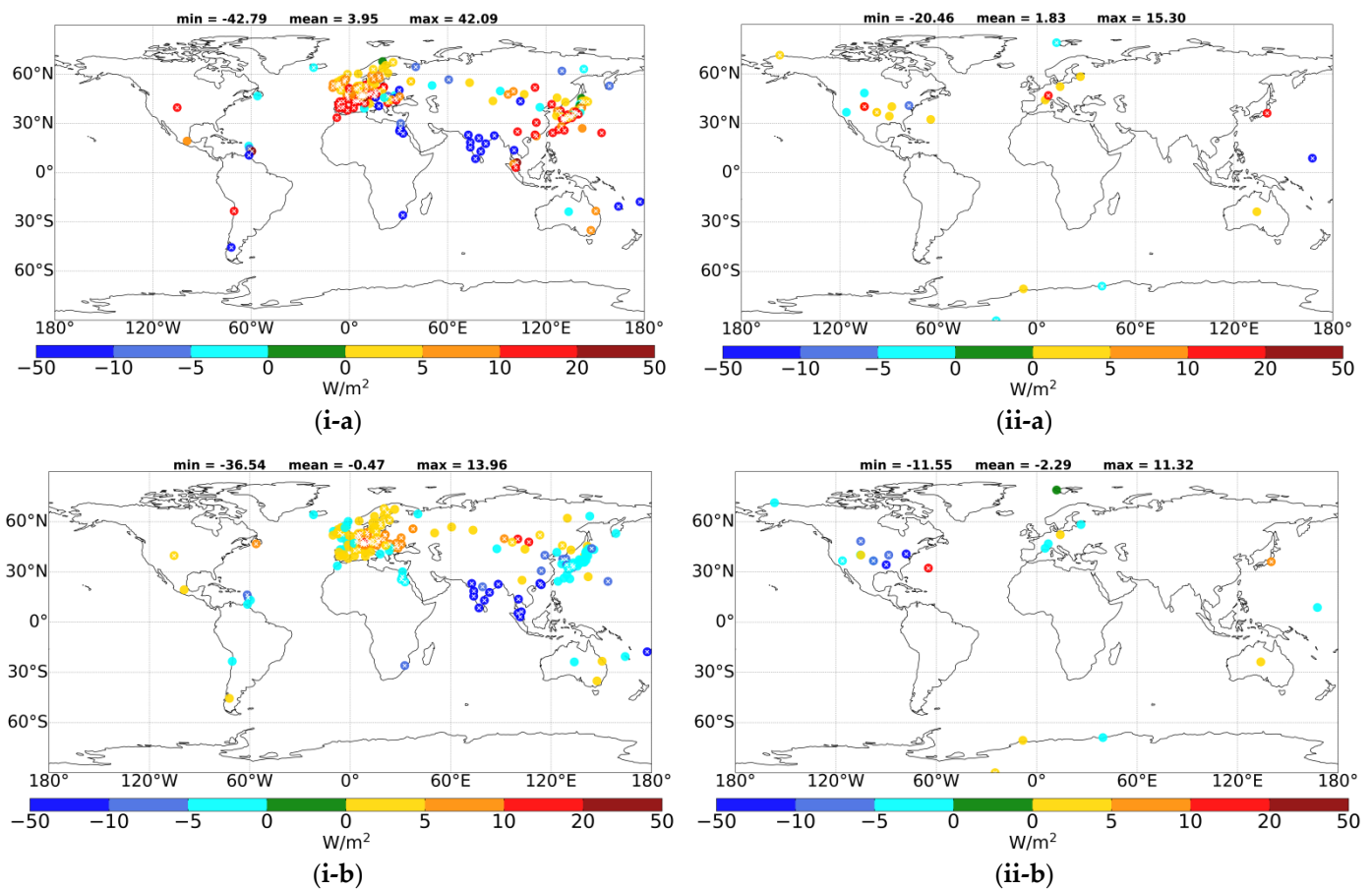


**Figure 8.** Computed GDB (or  $\Delta(SSR)$ , in  $W/m^2$ ) for GEBA (i-a) and BSRN (ii-a) stations and for the corresponding pixels of MERRA-2 containing the GEBA (i-b) and BSRN (ii-b) stations. Negative values, shown in blue and green colors, indicate dimming, and positive values, orange and red colors, indicate brightening. The embedded white x symbols indicate trends which are statistically significant (assessed at the 95% confidence level by applying the non-parametric Mann Kendall test). The trends are estimated over the periods covered by each station (shown in Figure S2).

According to the obtained trends of MERRA-2 pixels including the GEBA stations, over the same time period, the positive trends vary from 0.14 to 13.96  $W/m^2$ , and the negative trends from  $-0.05$  to  $-36.54$   $W/m^2$ , whereas the corresponding ranges for MERRA-2 pixels including the BSRN stations are 0.01–11.32 and  $-(0.00-11.55)$   $W/m^2$ . The MERRA-2 pixels including the GEBA sites, all together, indicate an average dimming of  $-0.47$   $W/m^2$  (Figure 8i-b), while the MERRA-2 pixels including the BSRN sites also indicate an even stronger dimming of  $-2.29$   $W/m^2$  (Figure 8ii-b), which are both of opposite sign to the corresponding GEBA/BSRN stations results. Yet, in spite of this average disagreement, there is partial agreement (for GEBA) between the respective average GDB computed only for cases, i.e., stations-pixels, with statistically significant trends. Specifically, the average MERRA-2 GDB for GEBA/BSRN sites is 0.51 and  $-3.45$   $W/m^2$ , while the corresponding mean GDB for GEBA/BSRN sites is 5.22 and 1.68  $W/m^2$ . Moreover, both MERRA-2 pixels and GEBA stations indicate strong and statistically significant dimming over India and strong brightening over Europe, with a stronger brightening occurring at the GEBA stations than MERRA-2. On the contrary, a clear disagreement, with GEBA brightening versus MERRA-2 dimming, is found over Japan, which explains the opposite overall sign of GDB between MERRA-2 pixels and GEBA sites reported above.

The priority in such a comparison between the MERRA-2 and GEBA/BSRN station-based trends of SSR, i.e., GDB, is the agreement/disagreement between their signs. This is better shown in Figure 9, which displays with blue/red bullets the stations for which



the trends of MERRA-2 and GEBA/BSRN stations SSR have the same/opposite sign. A satisfactory percentage of agreement (63.4%) between the signs of MERRA-2 and GEBA GDB is found, whereas the percentage is lower (50%) for BSRN stations. Furthermore, it is found that the percentage of agreement is somewhat better for cases (pixels) with statistically significant trends, being equal to 75.7% for GEBA and 66.7% for BSRN stations. The analysis using GEBA stations, which provide a relatively good spatial coverage over contiguous world areas, such as Europe, southern and eastern Asia or Australia, enables us to draw conclusions about systematic agreement/disagreement. Thus, it is found that in Europe, most stations (80.8%) show qualitative agreement, although there is a tendency of more frequent disagreement in coastal European regions. Besides, an absolute agreement, namely for all GEBA stations, is found over India and Australia. On the other hand, in Japan, most stations (86.1%) exhibit disagreement, while a mixed pattern (54.5% agreement) is found over Central Asia. Note that BSRN stations enable the coverage of North America, which was not possible with GEBA stations, where a mixed pattern appears, with agreement/disagreement in 5/5 (i.e., 50/50%) stations. It is interesting to note that in the present analysis, when using the values of the 22 selected BSRN stations, an agreement in the sign of GDB trends is found at 50% of stations, whereas using the total number (70) of BSRN stations, but without applying the strict availability criteria in the computation of SSR trends, agreement is found for more, i.e., 60%, stations. On the other hand, the corresponding percentage of agreement for all (1099) GEBA stations is 63.4%, i.e., equal to the percentage of 232 stations.

It is known that the MERRA-2 reanalysis products are better for years after 2000, because of the assimilation of modern state-of-the-art satellite data, such as Moderate Resolution Imaging Spectroradiometer (MODIS) and Multi-angle Imaging SpectroRadiometer (MISR), in the MERRA-2 Reanalysis System, resulting in more homogeneous time series [102]. Thus, the post 2000 period, namely 2000–2017, was selected in order to further and more thoroughly examine the quality of the MERRA-2 GDB. Additionally, in order to even more thoroughly examine the robustness of the MERRA-2 GDB, an additional analysis was undertaken to examine if MERRA-2 fluxes also provide a successful closure of the solar radiation budget. To this aim, specific GEBA/BSRN stations that provide agreement with MERRA-2 in terms of GDB were first selected. Subsequently, it was examined if for these stations the change of the MERRA-2 Outgoing Solar Radiation (OSR) at TOA agrees or not with the corresponding  $\Delta(\text{OSR})$  from CERES-EBAF satellite data, for the period 07/2000–06/2017. Successful closure for changing Earth SW radiation budget exists for those locations for which both  $\Delta(\text{SSR})$  and  $\Delta(\text{OSR})$  qualitatively agree with corresponding reference surface and satellite measurements. The signs of computed MERRA-2  $\Delta(\text{SSR})$  and  $\Delta(\text{OSR})$ , and the corresponding signs of GEBA/BSRN  $\Delta(\text{SSR})$  and CERES-EBAF  $\Delta(\text{OSR})$  are compared in Figure 10. At the surface, MERRA-2  $\Delta(\text{SSR})$  agrees with 62.5% of GEBA (145 out of 232) stations, and 31.8% BSRN (7 out of 22) stations. Then, the sign of  $\Delta(\text{OSR})$  between MERRA-2 and CERES was compared only for those stations providing agreement at the surface. In case of the 145 GEBA stations, qualitative agreement was found at TOA for 62.5% of them, which is encouraging. Respectively, for the 7 BSRN sites, agreement was found for 57.1% of them, which is a somewhat lower percentage than for GEBA. The obtained results for the comparison of MERRA-2 solar fluxes at the Earth's surface and TOA demonstrate that MERRA-2 cannot reasonably reproduce the changing SW radiation budget in the post 2000 period.



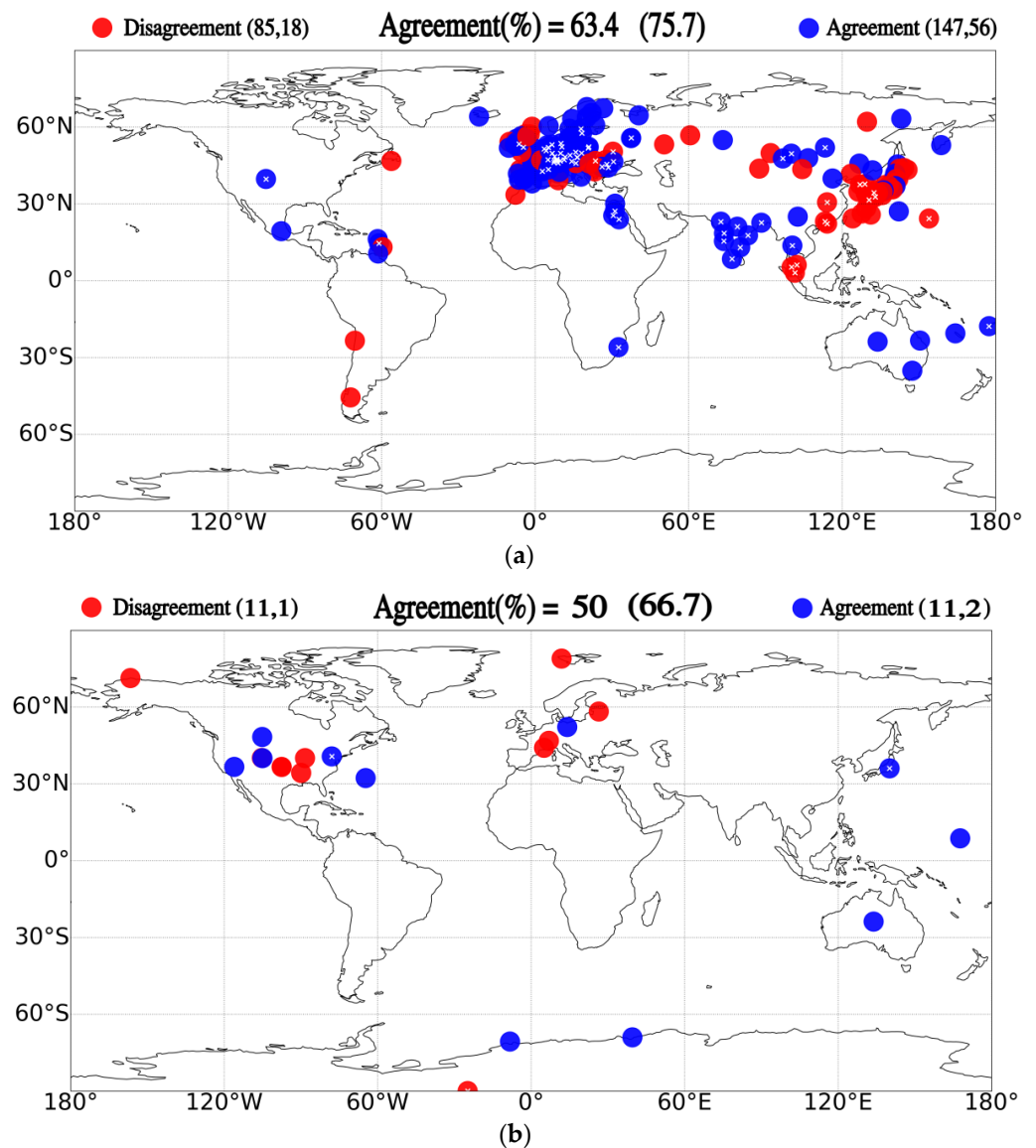
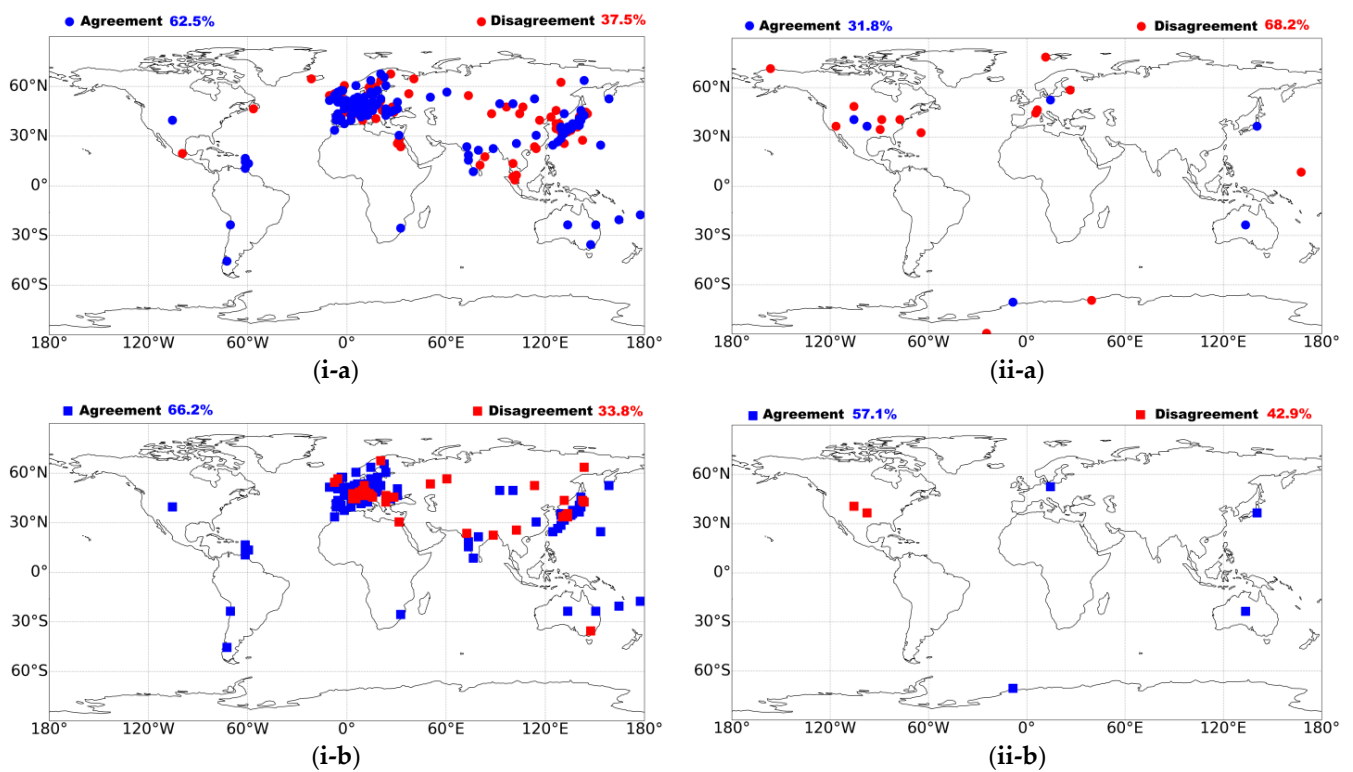


**Figure 9.** Agreement (blue dots) and disagreement (red dots) between trends of MERRA-2 and station deseasonalized SSR anomalies for GEBA (a) and BSRN (b) stations. The embedded white “x” symbols indicate the statistically significant trends for both MERRA-2 and stations. At the top left and top right parts above each panel figure, the numbers in parentheses provide the total number of stations for which there is agreement/disagreement (first number in parentheses) and the corresponding numbers for statistically significant trends (second number in parentheses). At the top center of each panel figure, the percent numbers of stations for which agreement, as well as those for which statistically significant agreement (in parenthesis), is found, are given.









The agreement/disagreement between the MERRA-2 and stations GDB has been also examined over specific sub-periods because, as reported in Section 1, the GDB undergoes decadal-scale changes. The selected sub-periods and the associated GDB patterns, according to the literature [11] based on station measurements, are: 1980–1985 (dimming), 1986–2000 (brightening), 2001–2010 (less brightening), and 2011–2020 (brightening & dimming). Time-series of deseasonalized anomalies of MERRA-2 and station SSR fluxes were created for each sub-period, to which a linear regression was applied and the Sen’s slope and, subsequently, the trends, namely the sign and magnitude of GDB, were computed. The GDB of the reanalysis and stations is compared either on individual station or on overall (all stations) basis and the results are given in Figure S6 and Tables 2 and 3, re-

spectively, emphasizing the agreement/disagreement between the sign of the computed average GDB from all stations and the corresponding MERRA-2 pixels. Overall (Table 2), qualitative agreement in terms of the GDB sign is found for 60.6% of the GEBA stations during 1980–1985, while the corresponding percentage is equal to 49.1% for 1986–2000, 58.6% for 2001–2010 and 74.2% for 2011–2017. With respect to the BSRN stations, agreement is found for 81.8% of stations in 1992–2000, 68.2% for 2001–2010 and 63.6% for 2011–2020. This analysis allows to assess possible inter-decadal changes in terms of agreement and probable improvement with time. Thus, the comparison with GEBA initially reveals a reasonable qualitative agreement during 1980–1985, which slightly deteriorates afterwards (1986–2000) and gradually improves from 2000 on. On the contrary, the comparison with BSRN shows initially (in the 1990s) a better agreement, which gradually deteriorates after 2000. Given that an improvement of agreement with time should be expected, due to the improving quality of MERRA-2 reanalysis with time, the absence of such an improvement for BSRN stations may be attributed to the small sample of stations (22) as well as to erroneous MERRA-2 fluxes at specific sites, as discussed above.









**Figure 10.** Agreement (blue dots) and disagreement (red dots) between trends of MERRA-2 and station deseasonalized SSR anomalies ( $\Delta(SSR)$ ), for GEBA (i-a) and BSRN (ii-a) stations for the period 07/2000–06/2017. The stations showing agreement at the surface against GEBA stations (i-a) and BSRN stations (ii-a), also having agreement of  $\Delta(OSR)$  with CERES at TOA, during the same period, are shown in (i-b) and (ii-b), respectively.

**Table 2.** Agreement between the GDB ( $\Delta(SSR)$ ) of MERRA-2 and GEBA stations over four different time periods. The percent number of GEBA stations for which same sign of GDB is found with the corresponding MERRA-2 pixels is given (in parentheses are the statistically significant trends), along with the average  $\Delta(SSR)$  and the number of stations/pixels with brightening and dimming (shown in parentheses) for both GEBA and MERRA-2. Red and blue vectors indicate Brightening and Dimming, respectively.

GEBA Periods	Agreement (%)	GEBA $\Delta(SSR)$ ( $W/m^2$ )	GEBA (BRI, DIM)	MERRA-2_pixel $\Delta(SSR)$ ( $W/m^2$ )	MERRA-2_pixel (BRI, DIM)
1980–1985	60.6 (75)	0.94 	(107, 101)	3.56 	(156, 52)
1986–2000	49.1 (47.4)	1.92 	(161, 71)	-1.33 	(108, 124)
2001–2010	58.6 (62.5)	0.19 	(135, 97)	-1.75 	(100, 132)
2011–2017	74.2 (80)	-1.68 	(70, 89)	-0.54 	(65, 94)

**Table 3.** As in Table 2, but for BSRN stations.

BSRN Periods	Agreement (%)	BSRN $\Delta(SSR)$ ( $W/m^2$ )	BSRN (BRI, DIM)	MERRA-2_pixel $\Delta(SSR)$ ( $W/m^2$ )	MERRA-2_pixel (BRI, DIM)
1992–2000	81.8 (0)	2.82 	(14, 8)	2.08 	(14, 8)
2001–2010	68.2 (0)	-0.89 	(9, 13)	-0.08 	(8, 14)
2011–2020	63.6 (0)	3.78 	(8, 14)	-2.43 	(6, 16)

In the first sub-period, i.e., 1980–1985, both GEBA and MERRA-2 indicate brightening (Table 2), albeit stronger for MERRA-2 ( $+3.56 W/m^2$ , resulting from 156/52 pixels with brightening/dimming) than GEBA ( $+0.94 W/m^2$ , resulting from 107/101 stations with brightening/dimming). It should be noted that the magnitude of the average GDB is not necessarily in line with the relative number of stations/pixels exhibiting brightening and dimming. This is not strange given that the magnitude of the average GDB is also driven by the magnitude of GDB at individual stations/pixels. Yet, the obtained agreement between the signs of average MERRA-2 and GEBA GDB in the first sub-period (1980–1985) is in line with the relatively high number of stations with agreement (60.6%). In contrast, during the next two sub-periods, i.e., 1986–2000 and 2001–2010, an opposite sign of GDB is found for GEBA (brightening equal to  $+1.92 W/m^2$  for 1986–2000 and  $+0.19 W/m^2$  for 2001–2010) and MERRA-2 (dimming equal to  $-1.33 W/m^2$  for 1986–2000 and  $-1.75 W/m^2$  for 2001–2010). Nevertheless, it should be noted that, actually, the disagreement for the period 2001–2010 is much weaker, and even uncertain, since the GEBA brightening is small and not significant, with values that are exceeded by the associated errors at the majority of GEBA stations (not shown here). This seems to be in line with the higher percent number (58.6%) of stations with agreement in 2001–2010 than the corresponding smaller number (49.1%) for 1986–2000. During the last sub-period, i.e., 2011–2017, both GEBA and MERRA-2 indicate dimming, which is stronger for GEBA ( $-1.68 W/m^2$ ) than for MERRA-2 ( $-0.54 W/m^2$ ). This agreement in sign of GDB is complemented by the high percent number of stations (74.2%) showing the same sign of GDB with the corresponding MERRA-2 pixels. Concerning the more problematic (in terms of agreement between the MERRA-2 and GEBA GDB) second sub-period, i.e., 1986–2000, our analysis shows (red circles in Figure S6i-b) that the overall disagreement largely arises from opposite GDB signs over Japan (disagreement in 41 out of 43 Japanese stations), a situation not found during the other three sub-periods. The reason for this disagreement can be attributed to problems with either MERRA-2 Reanalysis or the station measurements in Japan, which needs to be examined, but it is out of the scope of this study. Otherwise, no remarkable change, as it

concerns the agreement/disagreement on a regional scale, e.g., for Europe, is found from a sub-period to another.

As it concerns the comparison between the MERRA-2 and BSRN GDB in different sub-periods, there is a very good agreement in the first sub-period, i.e., 1992–2000, since both of them indicate brightening, which is  $+2.82 \text{ W/m}^2$  for BSRN resulting from 14/8 stations with brightening/dimming and for MERRA-2 is equal to  $+2.08 \text{ W/m}^2$  resulting from 14/8 pixels with brightening/dimming. During the next sub-period (2001–2010), the same sign of GDB is found either for BSRN (dimming equal to  $-0.89 \text{ W/m}^2$ ) and MERRA-2 (dimming equal to  $-0.08 \text{ W/m}^2$ ), though both they are not statistically significant. During the last sub-period (2011–2020), an agreement is found again between the Reanalysis' and BSRN stations' GDB. More specifically, the BSRN sites indicate a GDB equal to  $3.78 \text{ W/m}^2$ , resulting from 8/14 stations with brightening/dimming. It should be noted that the apparent contradiction of more stations with dimming resulting in a total brightening does not exist in practice, since the sign of GDB is not only determined by the number of stations with brightening/dimming, but also by the magnitude of brightening/dimming of each station. On the other hand, the corresponding MERRA-2 pixels indicate a dimming equal to  $-2.43 \text{ W/m}^2$  resulting from 6/16 stations with brightening/dimming. Thus, overall and during the entire period 1992–2020, it is found that MERRA-2 Reanalysis reproduces the phases of GDB (brightening and dimming) recorded by the BSRN station measurements. However, in spite of this agreement and the satisfactory global distribution of BSRN stations, their small number (unlike GEBA) does not allow us to continue using them in the next steps of this study focusing on the evaluation of MERRA-2 GDB on a regional level.

### 3.2.2. The MERRA-2 GDB on Global, Hemispherical and Regional Scales

The global distribution of MERRA-2 GDB, i.e.,  $\Delta(\text{SSR})$ , over the 40-year period 1980–2019 is given in Figure 11. Note that in this part of the analysis, which does not include comparison against stations, MERRA-2 data for 40 (instead of 37) years were utilized, since there is no restriction caused by the availability of GEBA/BSRN stations data. The computed  $\Delta(\text{SSR})$  values resulted from the application of linear regression to the time series of deseasonalized monthly MERRA-2 SSR anomalies for each pixel and the computation of the Sen's slope. Information about the statistical significance of GDB is also provided in the same figure (dotted colored pixels). According to MERRA-2, strong and statistically significant brightening (up to  $+32.9 \text{ W/m}^2$  or  $+0.826 \text{ W/m}^2/\text{year}$ ) is found over Europe, Central Africa, Mongolia, Mexico and some parts of the Tropical oceans, of Brazil and Argentina. In contrast, strong and statistically significant dimming (as strong as  $-57.38 \text{ W/m}^2$  or  $-1.435 \text{ W/m}^2/\text{year}$ ) is found over the western Tropical Warm Pool, India, Southeast China, Amazonia, stratocumulus covered areas and some parts of oceans such as over the mid-latitude Southern Hemisphere Ocean. No statistically significant trends were found over extended areas such as North America, Russia, Australia, Japan and Western Sahara. Opposite trends of SSR are found in neighboring areas over Africa, North and South America, Australia, Southeast Asia, eastern Tropical Warm Pool and the Mediterranean. Overall, solar dimming dominates (dimming in 62.8% of pixels versus brightening in 37.2% of pixels). According to our results, the computed tendencies of MERRA-2 SSR are statistically significant in 57% of pixels all over the globe; in those cells, i.e., over global areas with statistically significant GDB, solar dimming dominates even more, occurring in 81% of them. The overall dimming arises from global oceans (brightening/dimming in 27.7%/72.3% of pixels), while brightening slightly dominates over land (brightening/dimming occurring in 56.5%/43.5% of pixels). Additional information about the MERRA-2 GDB obtained on a seasonal basis (Figure S7) reveals seasonal variation of GDB features on a regional basis. For example, the annual brightening identified over Europe (Figure 11) is driven by a strong brightening in March–April–May and June–August, while a weaker brightening occurs in September–November, and mixed patterns are observed in December–February. Over the Southern Ocean, the stratocumulus-covered ocean areas off the western coasts of South



Africa and America, the Tropical Warm Pool, Amazonia and India, a systematic dimming is observed throughout the year, resulting in an annual dimming over these areas. Moreover, the dimming observed on an annual basis over Sahara (Figure 11), arises from a dimming throughout the year, being strongest in June–August, except for December–February when brightening occurs.

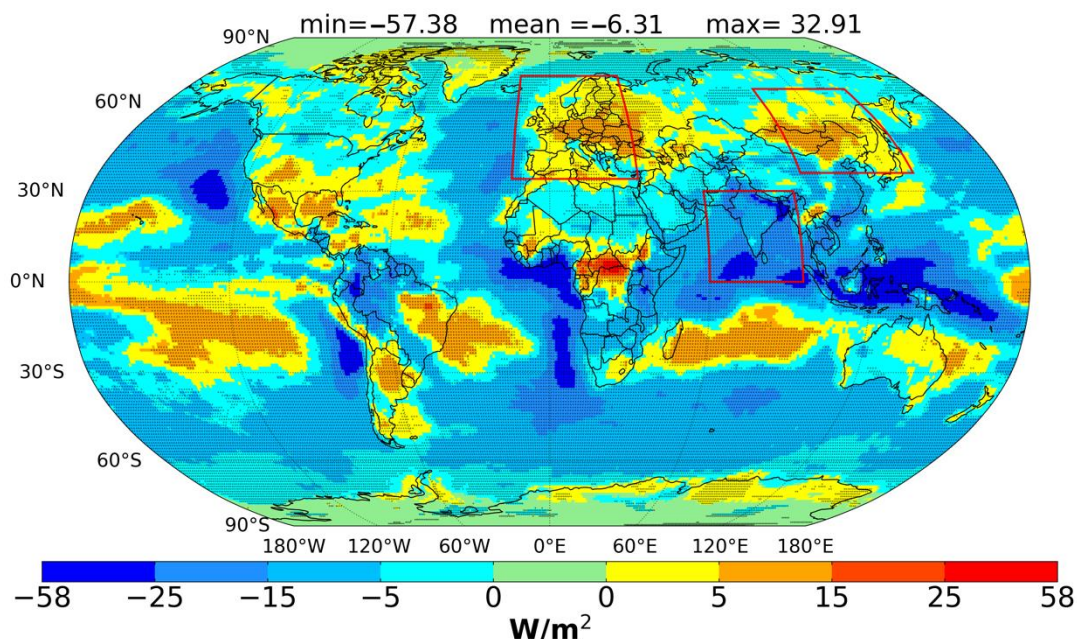


**Figure 11.** Global distribution of GDB, namely changes of MERRA-2 deseasonalized SSR anomalies, over the 40-year period January 1980–December 2019. Areas shaded with reddish/bluish colors are those with positive/negative trends (brightening/dimming). Areas (pixels) with statistically significant trends are indicated by black dots. World areas (Europe, India and East Asia) enclosed by red rectangles are characterized by homogeneous SSR trends (reference is made to them below).

Figure 12 displays the time series of the computed average deseasonalized SSR anomalies for the Globe, Northern Hemisphere and Southern Hemisphere over the 40-year period January 1980–December 2019. The MERRA-2 hemispherical SSR anomalies range from  $-8$  to  $10.52 \text{ W/m}^2$ , while the global mean SSR anomalies vary up to  $6.33 \text{ Wm}^{-2}$ . Large positive anomalies (brightening) are found during 1980–1991, while systematic negative anomalies, i.e., dimming, are observed during 2003–2019. This leads to an overall strong negative trend over the entire 1980–2019 period either over the Globe and the two hemispheres. Stronger positive anomalies occur in the SH than in the NH during 1980–1991, while after the Pinatubo eruption (1991) and through to 2019 larger negative anomalies occur again in the SH than in the NH. The 4th-order polynomial fit applied to the 40-year time-series shows a stronger decline of SSR during the period 1991–2008, against a stabilizing tendency of SSR afterwards. The decreasing SSR of MERRA-2 during 1991–2000 is not in agreement with most measurements and modelling studies [10,20,21,23], while during 2000–2009 this negative trend is in line with other studies [12,34,36]. MERRA-2 reproduces strong decreases of SSR, namely solar dimming, caused by the great volcano eruptions of El-Chichon (1982) and Pinatubo (1991), as well as by strong El-Nino's (e.g., 1998, 2004 and 2012). Years characterized by the El-Chichon and Pinatubo recovery, as well as La-Nina's (e.g., 2008, 2015 or 2018), are characterized by positive anomalies corresponding to brightening. These findings prove that MERRA-2 Reanalysis appropriately reproduces physical phenomena, such as volcanic eruptions and ENSO (El Nino Southern Oscillation), which drive the Earth's climate.

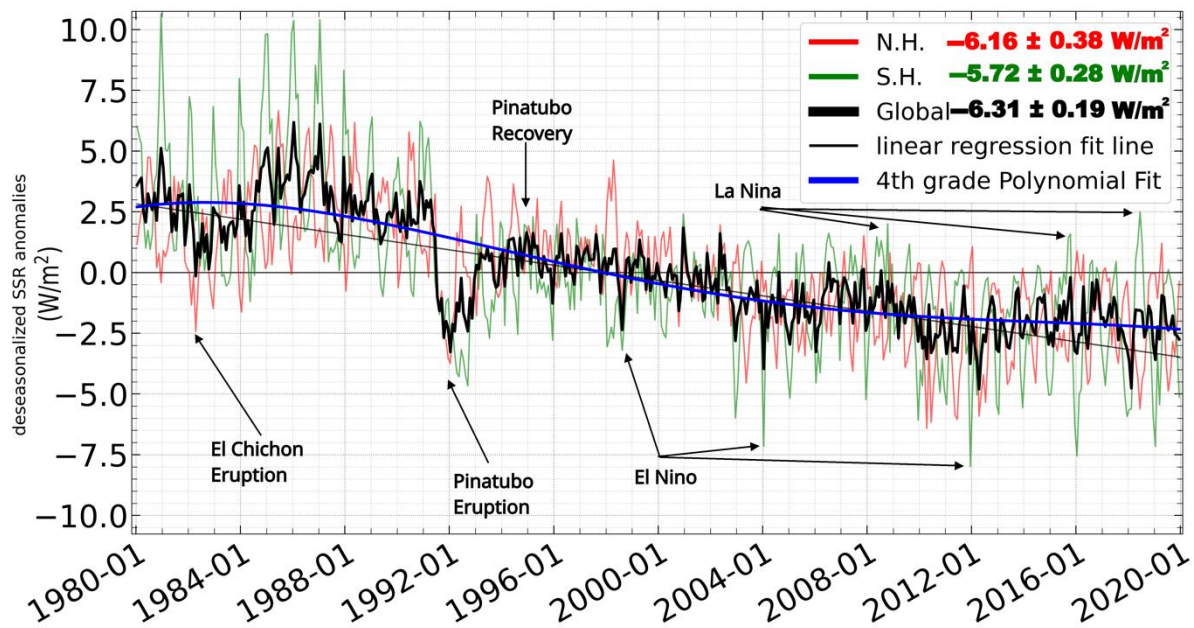


**Figure 12.** Timeseries of MERRA-2 average global (black line) and hemispherical (NH and SH, red and green lines) monthly mean deseasonalized SSR anomalies for the period January 1980–December 2019. Linear regression fit line, along with the associated  $\Delta(\text{SSR})$  for the Globe and the two hemispheres (numbers in the embedded panel), as well as the 4th-order polynomial fit applied to the global time series of MERRA-2 SSR, are also shown.

The MERRA-2 Reanalysis offers the advantage of covering a quite long (climatological) time period (1980–2019, i.e., 40 years) which overlaps with the recent anthropogenic global warming. There have been speculations, mostly based on surface station measurements of SSR, about how GDB interplays with this recent rapid global warming, either accelerating or counteracting it [8,18,22,103,104]. Therefore, the determination of GDB at these large spatial (global) and temporal (40-year) scales enables a better quantification and understanding of the role of GDB for the global warming, in relation to the predominant role of anthropogenic greenhouse gases, according to the MERRA-2 Reanalysis. To this aim, the changes of SSR, i.e., GDB, have been estimated not only over the entire 40-year period (1980–2019), but also over three sub-periods, January 1980–December 1999, January 2000–December 2009 and January 2010–December 2019, which have been characterized by different phases of GDB, according to the literature [11,12,24]. The results are given in Table 4 on global and hemispherical scales, as well as separately for land and oceans of the globe and the two hemispheres. According to MERRA-2, the SSR change during 1980–2019 is equal to  $-6.31 \pm 0.19 \text{ W/m}^2$  or  $-0.158 \pm 0.005 \text{ W/m}^2/\text{year}$  on global scale (dimming), with dimming observed in both hemispheres ( $-5.72 \pm 0.28$  and  $-6.16 \pm 0.38 \text{ W/m}^2$  or  $-0.143 \pm 0.007 \text{ W/m}^2/\text{year}$  and  $-0.154 \pm 0.01 \text{ W/m}^2/\text{year}$  over the North and South Hemispheres, respectively). Stronger dimming took place over oceans ( $-7.81 \pm 0.25 \text{ W/m}^2$  or  $-0.195 \pm 0.006 \text{ W/m}^2/\text{year}$ ) than continents ( $-2.58 \pm 0.25 \text{ W/m}^2$  or  $-0.065 \pm 0.006 \text{ W/m}^2/\text{year}$ ), which are in line with the stronger global warming observed over land than oceans ( $+0.29 \text{ }^\circ\text{C decade}^{-1}$  and  $+0.13 \text{ }^\circ\text{C decade}^{-1}$ , [105]). The overall 40-year dimming over the globe resulted from a persisting dimming from the early 1980's through to the late 2000's, being stronger in the 20th than in the 21st century, and a subsequent slight brightening from 2010 to 2019. The changing phases of GDB in the two hemispheres are the same as those already described for the globe, except for the last sub-period, i.e., 2010–2019, when brightening is found in MERRA-2 in the NH against dimming in SH. It is not the same with the land and oceanic areas of the two hemispheres, which have been characterized by different changing phases of GDB. Specifically, over the NH land, solar brightening took place during 1980–1999, followed by a dimming during

2000–2009 and 2010–2019. Over the global oceans, dimming persisted from 1980 to 2009, followed by a subsequent brightening from 2010 to 2019. It is found that, in general, but especially over oceans and the Southern Hemisphere, the magnitude of GDB is larger during the 20th century (1980–1999) than during the 21st century (2000–2019), which may be related to the assimilation of contemporary satellite data, such as MODIS, in the MERRA-2 Reanalysis. This change may point to a probably overestimated magnitude of GDB in this study estimated based on MERRA-2.

**Table 4.** Changes of MERRA-2 deseasonalized SSR anomalies ( $\Delta(\text{SSR})$ ), i.e., GDB, computed at global and hemispherical scales, as well as for land and ocean areas. Results are given for the entire 40-year period (1980–2019) as well as for three separate sub-periods. Red and blue vectors indicate solar brightening and dimming, respectively.

$\Delta(\text{SSR}) \pm \text{S.E.}$ ( $\text{W/m}^2$ )	January 1980–December 2019	January 1980–December 1999	January 2000–December 2009	January 2010–December 2019
Globe	$-6.31 \pm 0.19$	$-3.64 \pm 0.31$	$-1.19 \pm 0.26$	$0.44 \pm 0.24$
N.H.	$-5.72 \pm 0.28$	$-1.64 \pm 0.35$	$-1.92 \pm 0.35$	$0.39 \pm 0.37$
S.H.	$-6.16 \pm 0.38$	$-5.58 \pm 0.47$	$-0.33 \pm 0.46$	$-0.08 \pm 0.39$
Land-Globe	$-2.58 \pm 0.25$	$0.53 \pm 0.35$	$-2.45 \pm 0.38$	$0.25 \pm 0.39$
Land-N.H.	$-2.07 \pm 0.30$	$0.60 \pm 0.43$	$-2.44 \pm 0.48$	$-0.59 \pm 0.41$
Land-S.H.	$-2.98 \pm 0.42$	$0.36 \pm 0.53$	$-2.46 \pm 0.77$	$1.63 \pm 0.73$
Ocean-Globe	$-7.81 \pm 0.25$	$-5.29 \pm 0.35$	$-0.67 \pm 0.31$	$0.45 \pm 0.31$
Ocean-N.H.	$-8.06 \pm 0.38$	$-3.12 \pm 0.43$	$-1.45 \pm 0.43$	$1.16 \pm 0.54$
Ocean-S.H.	$-6.67 \pm 0.43$	$-6.88 \pm 0.54$	$0.16 \pm 0.53$	$-0.44 \pm 0.45$

It should be noted that in the NH the MERRA-2 brightening phase of 2010–2019 and the dimming in 2000–2009 harmonize with the stronger global warming ( $+0.47 \text{ }^\circ\text{C decade}^{-1}$ ) recorded in the second decade of the 21st century and the weaker warming ( $+0.16 \text{ }^\circ\text{C decade}^{-1}$ ) observed in the first decade [105]. Furthermore, it should be noted that the MERRA-2 dimming during the 1980s and 1990s may have resulted in a slower rate of NH warming in this period ( $+0.2 \text{ }^\circ\text{C decade}^{-1}$ ) than in the 2010s when a brightening occurred. Moreover, it is found that the brightening phases during 1980–1999 and 2010–2019, and the dimming in 2000–2009, over the land areas of the globe match with the rapid warming in the 1980s, 1990s and 2010s and the recent hiatus in the 2000s. These results indicate that the MERRA-2 GDB phases are in line with the NH warming rates, since brightening/dimming accelerates/decelerates warming. However, this is not valid when looking at the NH land and ocean areas separately, since the MERRA-2 dimming over NH land in 2010–2019 is not in line with the strong warming ( $+0.46 \text{ }^\circ\text{C decade}^{-1}$ ) during this period. On the other hand, in the SH, there is no clear relationship between the MERRA-2 GDB phases and the recorded warming rates. These results, which underline the role of GDB for the global temperatures in relation with the greenhouse warming, corroborate the findings of [11], who using the 2-m temperature dataset from the Climate Research Unit of the University of East Anglia (HadCRUT4 (Hadley Centre of the UK Met Office by the Climatic Research Unit)), suggested that in the polluted NH, during the dimming phase in the period 1950s–1980s, which was characterized by a strong increase of aerosol loadings, no warming has been observed, while during the subsequent brightening phase (1980s–2000s) characterized by decreasing aerosol loadings, a rapid warming was observed. In contrast, in the more pristine SH, where greenhouse-gases is the sole major anthropogenic forcing, warming is observed during both dimming and brightening phases.



Given that GDB is a regional phenomenon (Figure 11), and that the 40-year GDB results in Figures 11 and 12 are based on linear trending analysis, an additional investigation was performed on a regional scale, in order to reveal decadal scale GDB features. To this aim, three specific regions of the Globe were selected, which have a satisfactory coverage by stations and exhibit homogeneous GDB patterns (Figure 11). These regions, shown in rectangles in Figure 11, are the land areas of Europe, East Asia and India. Three time series of deseasonalized SSR anomalies (for the period January 1980–December 2019) were produced for the selected world regions, one for the GEBA stations lying in each region (125 stations in Europe, 36 in E. Asia and 8 in India) that satisfy the 2 criteria of slope estimation as mentioned in Section 2.2, a second one of the respective MERRA-2 pixels (including the stations) of the region, and a third one of all MERRA-2 pixels of the region and are shown in Figure 13. Along with the time series, the corresponding applied linear regression and computed trends are also given. This analysis allows testing the ability of MERRA-2 to reproduce the inter-annual variability and trend of SSR at the locations of GEBA stations within each region, as well as examining whether the station (or corresponding pixel areas) based trends of SSR are representative for the entire areas of Europe, India and East Asia. In general, it is found that MERRA-2 satisfactorily reproduces the month-to-month and year-to-year variability of SSR (correlation coefficients equal to 0.88, 0.77 and 0.66, for Europe, East Asia and India, respectively), although GEBA measurements exhibit a slightly larger variability, especially for Europe and East Asia. For India, it is found that GEBA measurements indicate distinct negative SSR anomalies during the decade 2010–2019, against quite smaller, still negative, anomalies for MERRA-2. On the other hand, large positive GEBA SSR anomalies are found for East Asia during the decade 2010–2019, against smaller positive anomalies for MERRA-2. As a result of these discrepancies, a stronger decreasing trend of SSR, i.e., a stronger dimming, is found for India according to GEBA ( $-33.81 \text{ W/m}^2$ ) than corresponding MERRA-2 pixels ( $-17.97 \text{ W/m}^2$ ), as well as a larger increasing GEBA-based trend of SSR, i.e., stronger brightening, for East Asia ( $+5.31 \text{ W/m}^2$ ) than corresponding MERRA-2 pixels ( $+0.37 \text{ W/m}^2$ ). On the other hand, the trends for Europe are about equal ( $+6.86$  and  $+4.03 \text{ W/m}^2$  according to GEBA and MERRA-2 pixels, respectively), indicating brightening in both cases. With respect to the representativeness of the station (or corresponding MERRA-2 pixels) based SSR trends for the entire world regions, it is found that, indeed, they are, since there is a similarity between the sign of their trends, both showing the same phases of GDB. In addition, a great similarity is also found in terms of magnitude of GDB's for East Asia and India, with slight differences for Europe, where there is a slightly smaller trend for the entire region ( $+1.78 \text{ W/m}^2$ ) than for the MERRA-2 pixels ( $+4.03 \text{ W/m}^2$ ) and GEBA stations ( $+6.86 \text{ W/m}^2$ ). Our results prove the ability of MERRA-2 to qualitatively reproduce the GEBA stations-based GDB (dimming or brightening) over the continental areas of Europe, East Asia and India. Moreover, they also indicate that the GDB based on measurements of GEBA stations in East Asia and India can be considered as representative for the entire areas to a high degree, but this is not entirely valid for Europe. The MERRA-2-based time series for Europe, India and East Asia enable to assess the inter-decadal changes of SSR occurring over these three world regions characterized by significant anthropogenic activities. The obtained results reveal that over Europe (continental areas) a brightening occurred from 1980 to 2000, in agreement with other studies ([22] and references therein), which reversed to weak dimming beyond 2000, which rather agrees with [106] who suggested a tendency of stabilization of SSR since the early 21st century. Over India, a considerable brightening took place from 1980 to 1985, followed by a dimming till 2010 (in agreement with [107]) and a subsequent brightening till 2019. In East Asia, a brightening occurred from 1980 to 2000, in agreement with [26], which was succeeded by a slight dimming through to 2014. This slight dimming is in line with the reported decline of the rate of increase of SSR in the 2000s by [24] and has been followed by a brightening after 2014.



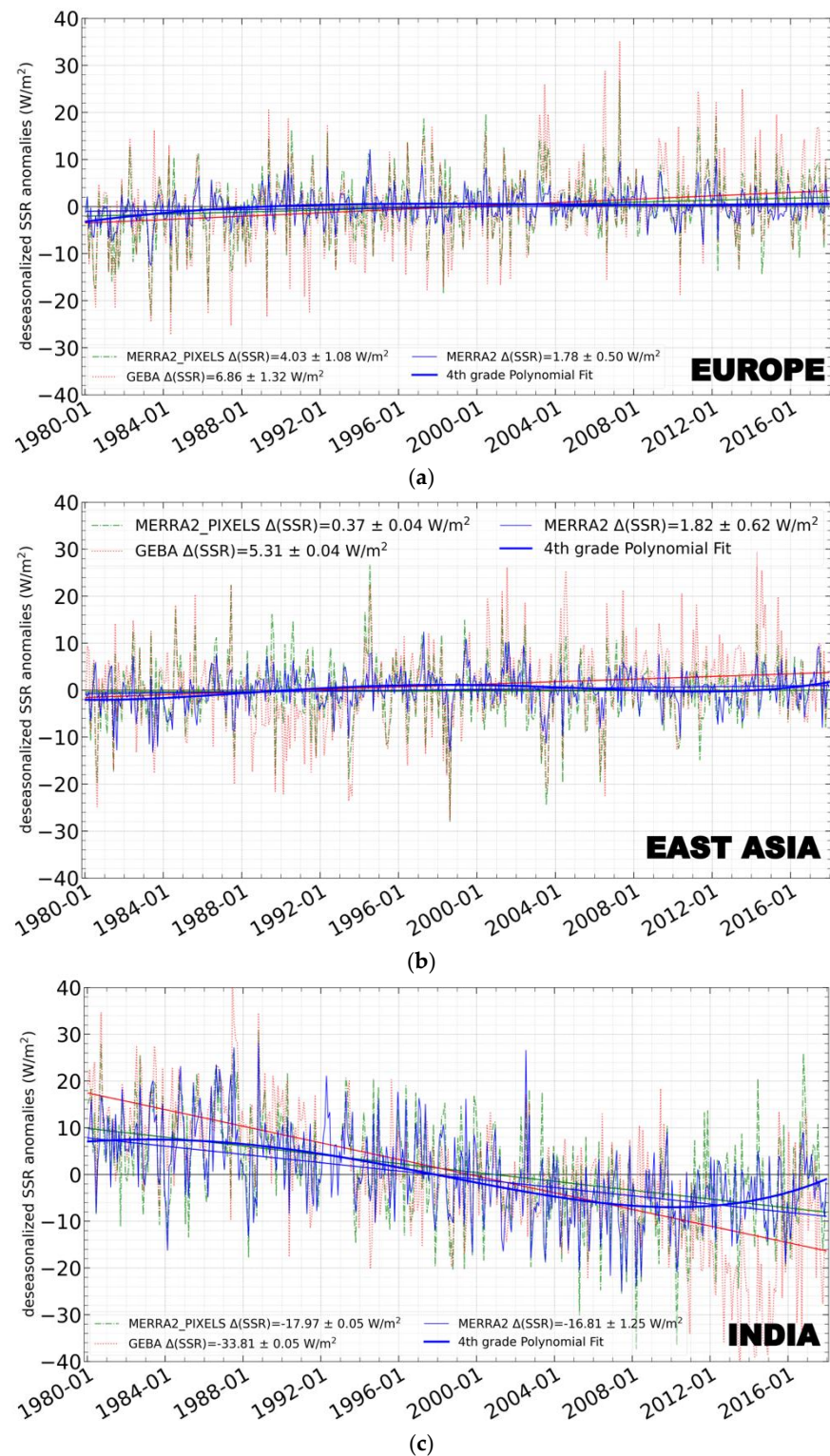


**Figure 13.** Timeseries (January 1980–December 2017) of deseasonalized anomalies of SSR for three selected world areas with homogeneous trends (see red rectangles in Figure 11), namely, Europe (a), East Asia (b) and India (c). For every area, results are given based on GEBA stations (red dotted lines), corresponding MERRA-2 pixels (including the stations, green dot-dashed lines) and all MERRA-2 pixels of the areas (blue lines). Moreover, the linearly fitted lines to each timeseries are also displayed with similar colors, while blue line displaying the 4th-order polynomial fit applied to the time series of MERRA-2 SSR for the entire world areas are also shown.

#### 4. Conclusions

Reanalysis datasets have the advantage of providing global coverage and long-term data for various climate parameters, including SSR. Yet, the reanalysis data assimilation can lead to errors in SSR and its interannual variation and trends and, hence, in uncertainties in studies making use of them. Therefore, before applying reanalysis SSR products in climate studies, it is necessary to validate them against available reference ground measurements. A detailed and thorough evaluation and verification of MERRA-2 reanalysis SSR for the 40-year period 1980–2019 has been performed here against ground measurements and satellite estimates at scales ranging from global, to regional and down to local (station-level). In particular, this study deals, for the first time to our knowledge, with the detailed evaluation of MERRA-2 SSR and their changes ( $\Delta(\text{SSR})$  or GDB) over the period 1980–2019 using high-quality surface measurements from 1099 GEBA and 70 BSRN stations. The performed analysis enabled to derive some useful conclusions, which are summarized as follows.

- The MERRA-2 SSR fluxes correlate very well with the ground truth measurements, with R values equal to 0.95 and 0.97 for the comparison with GEBA and BSRN stations, respectively. The corresponding R values for the comparison of deseasonalized SSR anomalies, which are free of the seasonal cycle and give more meaningful results, are still satisfactory and equal to 0.61 and 0.62. On an individual station-level, the estimated R values range from  $-0.25$  to  $0.92$ , the lowest values occurring in tropical and sub-tropical regions, probably due to uncertainties in the Reanalysis cloudiness.
- In general, there is an overestimation of MERRA-2 SSR compared to GEBA and BSRN measurements, the mean bias being equal to  $24.25$  and  $10.31 \text{ W/m}^2$  or  $15.3$  and  $5.9\%$ , respectively. The ranges of variability of the biases in terms of absolute and relative percent values for individual stations are  $-64.24$ – $141.07 \text{ W/m}^2$  or  $-20.3$ – $103.9\%$  for GEBA and  $-36.32$ – $54.97 \text{ W/m}^2$  or  $-15.8$ – $35\%$  for BSRN stations. However, MERRA-2 underestimates SSR at low latitudes and polar regions. The general overestimation leads to the conclusion that the atmosphere of MERRA-2 is too transparent. The computed average RMSE is equal to  $36.07 \text{ W/m}^2$  (equivalent to  $22.8\%$ ) for the comparison of MERRA-2 with GEBA, while the corresponding values for BSRN are equal to  $26.12 \text{ W/m}^2$  or  $15.1\%$ . The RMSE values are high in the tropics and the highest in Southern China.
- The assessment of the performance of MERRA-2 SSR with GEBA on a seasonal basis has shown that in both hemispheres the performance is worse during the cold period of the year, when the computed hemispherical mean values of percent bias and RMSE are the highest ( $17.9$  and  $30.9\%$ , respectively) and those of R are the lowest ( $0.52$ ).
- The time-series of the average SSR anomalies of GEBA and BSRN stations and the corresponding MERRA-2 pixels show that MERRA-2 show larger anomalies, positive before 2000 and negative in the post 2000 years, which can affect the computed trends of SSR, namely GDB, of MERRA-2 and stations. Indeed, the MERRA-2 SSR trends show a stronger dimming and a weaker brightening than the stations' trends.
- Comparing the sign of GDB for each station (232 GEBA and 22 BSRN) and MERRA-2 pixels where the stations are located, an agreement is found for  $63.4\%$  of matched MERRA-2 and GEBA pairs (for the period 1980–2017), with the corresponding number being equal to  $50\%$  for the matched MERRA-2 and BSRN pairs (for the period 1992–2020). A very good agreement between the Reanalysis and stations in terms of signs of GDB is found for Europe and India, opposite to a strong disagreement in Japan.
- The estimated MERRA-2 SSR changes (GDB) during the 40-year period 01/1980–12/2019, reveal a statistically significant brightening in Europe, Central Africa, Mongolia, Mexico, parts of the tropical oceans, Brazil and Argentina. In contrast, statistically significant dimming is found over the western Tropical Warm Pool, India, Southern East China, Amazonia, stratocumulus covered marine areas off the western coasts of Africa and America and some parts of oceans.

- Globally, MERRA-2 SSR shows a dimming (decreasing SSR) from 1980 to 2019, equal to  $-6.31 \pm 0.19 \text{ W/m}^2$  or  $-0.158 \pm 0.005 \text{ W/m}^2/\text{year}$ , with 62.8% of the global MERRA-2 geographic cells showing dimming. This dimming is found over both land and ocean areas of the globe, but oceans underwent a stronger dimming ( $-7.81 \pm 0.25 \text{ W/m}^2$  or  $-0.195 \pm 0.006 \text{ W/m}^2/\text{year}$ ) than land ( $-2.58 \pm 0.25 \text{ W/m}^2$  or  $-0.065 \pm 0.006 \text{ W/m}^2/\text{year}$ ). Solar dimming also occurred on hemispherical basis, being stronger in the Southern than Northern Hemisphere ( $-5.72 \pm 0.28 \text{ W/m}^2$  versus  $-6.16 \pm 0.38 \text{ W/m}^2$  or  $-0.143 \pm 0.007 \text{ W/m}^2/\text{year}$  versus  $-0.154 \pm 0.01 \text{ W/m}^2/\text{year}$ , respectively).
- Examining possible changes of the agreement between the signs of GDB of GEBA stations and MERRA-2 with time, an improvement is found since 1985, and especially in the post-2000 period, which can be related to the assimilation of state-of-the-art satellite data (MODIS, MISR) in MERRA-2 after 2000.
- During the reported brightening in the literature in the 1980s and 1990s, MERRA-2 reproduces brightening only over land, which is in line with the rapid global warming in the North Hemisphere driven by anthropogenic greenhouse gases. In the 2000s, when a recent hiatus has been recorded, MERRA-2 indicates a dimming both on a global basis ( $-1.19 \pm 0.26 \text{ W/m}^2$  or  $-0.119 \pm 0.026 \text{ W/m}^2/\text{year}$ ) and on a hemispherical one, which seems to be in line with the deceleration of global warming. In the 2010s, MERRA-2 suggests a weak global brightening ( $+0.44 \pm 0.24 \text{ W/m}^2$  or  $+0.044 \pm 0.024 \text{ W/m}^2/\text{year}$ ), which is in accord with the recurring accelerated warming of the Globe. Thus, overall, the MERRA-2 GDB phases, especially in the Northern Hemisphere, seem to be consistent with the accelerating and decelerating decadal phases of global warming since 2000.

Overall, the present study, based on detailed comparisons against the reference global GEBA and BSRN station networks, documents a quite satisfactory performance of the MERRA-2 SSR, along with a worse performance of MERRA-2 SSR changes during the 40-year period 1980–2019. These results at the Earth's surface are accompanied by a less satisfactory comparison of the corresponding to SSR top of atmosphere solar fluxes of MERRA-2 against reference CERES fluxes. The ascertained performance of MERRA-2 SSR data is encouraging towards their use in various climate studies, but they cannot provide reliable SSR trends and GDB assessment. In conclusion, further improvements to MERRA Reanalysis solar fluxes are necessary, which are, however, worth given the advantages of this Reanalysis, like its complete spatial (global) and long temporal (climatological) coverage and the consideration, for the first time, of aerosol-cloud interactions. With the expected continuation and extension of the MERRA Reanalysis in the time to come, an even longer climatology of SSR will be created, which will enable a better assessment of the climatic role of the GDB phenomenon, especially in relation with the ongoing greenhouse warming. However, such assessments can only be reliable by making additional improvements to the MERRA-2 SSR products.

**Supplementary Materials:** The following supporting information can be downloaded at: <https://www.mdpi.com/article/10.3390/app121910176/s1>, Figure S1: Global distribution of: (a) Global Energy Balance Archive (GEBA) 1397 stations and (b) Baseline Surface Radiation Network (BSRN) 73 stations, whose surface solar radiation (SSR) data (availability in years indicated in the colorbars) have been used in the study; Figure S2: Time periods covered by measurements of each station for (i) GEBA and (ii) BSRN networks. (a) Total number of stations since 1980 and (b) Number of available stations after applying criteria to compute linear slopes, i.e., 232 GEBA and 22 BSRN stations; Figure S3: Seasonal variation of hemispherical mean correlation coefficient R between MERRA-2 and GEBA (blue color) and between MERRA-2 and BSRN (red color) stations, computed using SSR fluxes for the North Hemisphere (i) and the South Hemisphere (ii); Figure S4: Global distribution of correlation coefficient between MERRA-2 and each GEBA (i, left column) and BSRN (ii, right column) station SSR fluxes; Figure S5: Histogram of frequency distribution of correlation coefficient R (a), bias (b), relative bias (c), root mean squared error (RMSE) (d), relative RMSE (e), between MERRA-2 and GEBA (i, left column) and BSRN (ii, right column) stations. Results are computed

using MERRA-2, and GEBA and BSRN station SSR fluxes, except for R, which is computed using deseasonalized SSR anomalies. In the left y axis shown is given the number of stations, while in the right y axis the % number of stations; Figure S6: Agreement (blue dots) and disagreement (red dots) between trends of MERRA-2 and station SSR fluxes. The comparison is done for the associated deseasonalized anomalies for GEBA (left column, i) and BSRN (right column, ii) stations per selected time periods that are characterized as Global Dimming & Brightening periods (GDB phases). The embedded white x symbols indicate the statistically significant trends. The numbers in parentheses provide the total number of stations for which there is agreement/disagreement (first number) and the corresponding numbers for statistically significant trends (second number). The GDB phases (Wild et al., WIREsClim Change 2016, 7:91-107) are: (a) 1980–1985, (b) 1986–2000, (c) 2001–2010, (d) 2011–2017 for GEBA and (a) 1992–2000, (b) 2001–2010, (c) 2011–2020 for BSRN. Figure S7: Global distribution of MERRA-2  $\Delta(\text{SSR})$  anomalies over the 40-year period January 1980–December 2019, for (a) DJF, (b) MAM, (c) JJA, (d) SON. Reddish colors are those with positive trends (brightening), and those with bluish colors have negative trends (dimming). Statistically significant trends are indicated by black dots.

**Author Contributions:** Conceptualization, N.H.; methodology, N.H. and M.S.; software, N.H., M.S. and M.B.K.-C.; validation, N.H., M.S. and M.B.K.-C.; formal analysis, M.S.; investigation, N.H. and M.S.; resources, N.H.; data curation, M.S.; writing—original draft preparation, M.S.; writing—review and editing, N.H., M.S., M.B.K.-C., M.W., I.V. and C.M.; visualization, M.S. and M.B.K.-C.; supervision, N.H.; project administration, N.H.; funding acquisition, N.H. All authors have read and agreed to the published version of the manuscript.

**Funding:** This research received no external funding.

**Institutional Review Board Statement:** Not applicable.

**Informed Consent Statement:** Not applicable.

**Data Availability Statement:** Not applicable.

**Acknowledgments:** We acknowledge support of this work by the project “Dioni: Computing Infrastructure for Big-Data Processing and Analysis.” (MIS No. 5047222) which is implemented under the Action “Reinforcement of the Research and Innovation Infrastructure”, funded by the Operational Programme “Competitiveness, Entrepreneurship and Innovation” (NSRF 2014–2020) and co-financed by Greece and the European Union (European Regional Development Fund). Global dimming and brightening research at ETH Zürich got support from a sequence of Swiss National Science Foundation Grants (Grant Nos. 200021\_135395, 200020\_159938, 200020\_188601). GEBA is co-funded by the Federal Office of Meteorology and Climatology MeteoSwiss within the framework of GCOS Switzerland.

**Conflicts of Interest:** The authors declare no conflict of interest.

## Abbreviations

MERRA-2	Modern-Era Retrospective Analysis for Research and Applications v.2
GEBA	Global Energy Balance Archive
BSRN	Baseline Surface Radiation Network
SSR	Surface Solar Radiation
$\Delta(\text{SSR})$	change of SSR (equivalent to GDB)
GDB	Global Dimming and Brightening
R	Pearson’s correlation coefficient
BIAS	mean value of MERRA-2 minus mean value of stations
BIAS (%)	$100 \cdot \text{BIAS} / \text{mean value of stations}$
RMSE	Root Mean Squared Error
RRMSE	Relative Root Mean Squared Error
M	mean value of MERRA-2
M <sub>i</sub>	monthly (for the -i month) value of MERRA-2
G	mean value of stations
G <sub>i</sub>	monthly (for the -i month) value of stations
n	number of monthly data



TOA	Top of the Atmosphere
OSR	Outgoing Solar Radiation
$\Delta$ (OSR)	Changes of OSR
NH	Northern Hemisphere
SH	Southern Hemisphere

## References

- Besharat, F.; Dehghan, A.A.; Faghih, A.R. Empirical Models for Estimating Global Solar Radiation: A Review and Case Study. *Renew. Sustain. Energy Rev.* **2013**, *21*, 798–821. [\[CrossRef\]](#)
- Wang, Y.; Yang, K.; Pan, Z.; Qin, J.; Chen, D.; Lin, C.; Chen, Y.; Tang, W.; Han, M.; Lu, N.; et al. Evaluation of Precipitable Water Vapor from Four Satellite Products and Four Reanalysis Datasets against GPS Measurements on the Southern Tibetan Plateau. *J. Clim.* **2017**, *30*, 5699–5713. [\[CrossRef\]](#)
- López, G.; Rosales, S.; Gueymard, C.; Marzo, A.; Alonso-Montesinos, J.; Polo, J.; Martin Chivelet, N.; Ferrada, P.; Batlles, F.; Vela, N.; et al. Effect of Cloudiness on Solar Radiation Forecasting. In *Solar Energy Resource Management for Electricity Generation from Local Level to Global Scale*; Nova Science Publishers: New York, NY, USA, 2019; pp. 1–11.
- Luo, H.; Ge, F.; Yang, K.; Zhu, S.; Peng, T.; Cai, W.; Liu, X.; Tang, W. Assessment of ECMWF Reanalysis Data in Complex Terrain: Can the CERA-20C and ERA-Interim Data Sets Replicate the Variation in Surface Air Temperatures over Sichuan, China? *Int. J. Climatol.* **2019**, *39*, 5619–5634. [\[CrossRef\]](#)
- Wild, M. Enlightening Global Dimming and Brightening. *Bull. Am. Meteorol. Soc.* **2012**, *93*, 27–37. [\[CrossRef\]](#)
- Yang, E.-G.; Kim, H.M. Evaluation of Short-Range Precipitation Reforecasts from East Asia Regional Reanalysis. *J. Hydrometeorol.* **2019**, *20*, 319–337. [\[CrossRef\]](#)
- Yeom, J.-M.; Deo, R.; Adamowski, J.; Park, S.; Lee, C.S. Spatial Mapping of Short-Term Solar Radiation Prediction Incorporating Geostationary Satellite Images Coupled with Deep Convolutional LSTM Networks for South Korea. *Environ. Res. Lett.* **2020**, *15*, 094025. [\[CrossRef\]](#)
- Philipona, R.; Behrens, K.; Ruckstuhl, C. How Declining Aerosols and Rising Greenhouse Gases Forced Rapid Warming in Europe since the 1980s. *Geophys. Res. Lett.* **2009**, *36*, L02806. [\[CrossRef\]](#)
- Wang, Y.; Wild, M. A New Look at Solar Dimming and Brightening in China. *Geophys. Res. Lett.* **2016**, *43*, 777–785. [\[CrossRef\]](#)
- Hatzianastassiou, N.; Matsoukas, C.; Fotiadi, A.; Pavlakis, K.G.; Drakakis, E.; Hatzidimitriou, D.; Vardavas, I. Global Distribution of Earth's Surface Shortwave Radiation Budget. *Atmos. Chem. Phys.* **2005**, *5*, 2847–2867. [\[CrossRef\]](#)
- Wild, M. Decadal Changes in Radiative Fluxes at Land and Ocean Surfaces and Their Relevance for Global Warming. *WIREs Clim. Chang.* **2016**, *7*, 91–107. [\[CrossRef\]](#)
- Hatzianastassiou, N.; Ioannidis, E.; Korras-Carraca, M.-B.; Gavrouzou, M.; Papadimas, C.D.; Matsoukas, C.; Benas, N.; Fotiadi, A.; Wild, M.; Vardavas, I. Global Dimming and Brightening Features during the First Decade of the 21st Century. *Atmosphere* **2020**, *11*, 308. [\[CrossRef\]](#)
- Greenwald, R.; Bergin, M.H.; Xu, J.; Cohan, D.; Hoogenboom, G.; Chameides, W.L. The Influence of Aerosols on Crop Production: A Study Using the CERES Crop Model. *Agric. Syst.* **2006**, *89*, 390–413. [\[CrossRef\]](#)
- Roderick, M.L.; Farquhar, G.D. Hazy, Cool and Well Fed? *Nat. Clim. Chang.* **2012**, *2*, 76–77. [\[CrossRef\]](#)
- Gupta, R.; Somanathan, E.; Dey, S. Global Warming and Local Air Pollution Have Reduced Wheat Yields in India. *Clim. Chang.* **2017**, *140*, 593–604. [\[CrossRef\]](#)
- Wild, M.; Roesch, A.; Ammann, C. Global Dimming and Brightening—Evidence and Agricultural Implications. *CABI Rev.* **2012**, *2012*, 1–7. [\[CrossRef\]](#)
- Liepert, B.; Romanou, A. Global Dimming and Brightening and the Water Cycle. *Bull. Am. Meteorol. Soc.* **2005**, *86*, 622–623.
- Wild, M.; Ohmura, A.; Makowski, K. Impact of Global Dimming and Brightening on Global Warming. *Geophys. Res. Lett.* **2007**, *34*, L04702. [\[CrossRef\]](#)
- Gilgen, H.; Wild, M.; Ohmura, A. Means and Trends of Shortwave Irradiance at the Surface Estimated from Global Energy Balance Archive Data. *J. Clim.* **1998**, *11*, 2042–2061. [\[CrossRef\]](#)
- Stanhill, G.; Cohen, S. Global Dimming: A Review of the Evidence for a Widespread and Significant Reduction in Global Radiation with Discussion of Its Probable Causes and Possible Agricultural Consequences. *Agric. For. Meteorol.* **2001**, *107*, 255–278. [\[CrossRef\]](#)
- Liepert, B.G. Observed Reductions of Surface Solar Radiation at Sites in the United States and Worldwide from 1961 to 1990. *Geophys. Res. Lett.* **2002**, *29*, 61-1–61-4. [\[CrossRef\]](#)
- Wild, M. Global Dimming and Brightening: A Review. *J. Geophys. Res. Atmos.* **2009**, *114*, D00D16. [\[CrossRef\]](#)
- Wild, M.; Gilgen, H.; Roesch, A.; Ohmura, A.; Long, C.N.; Dutton, E.G.; Forgan, B.; Kallis, A.; Russak, V.; Tsvetkov, A. From Dimming to Brightening: Decadal Changes in Solar Radiation at Earth's Surface. *Science* **2005**, *308*, 847–850. [\[CrossRef\]](#)
- Wild, M.; Trüssel, B.; Ohmura, A.; Long, C.N.; König-Langlo, G.; Dutton, E.G.; Tsvetkov, A. Global Dimming and Brightening: An Update beyond 2000. *J. Geophys. Res. Atmos.* **2009**, *114*, D00D13. [\[CrossRef\]](#)
- Norris, J.R.; Wild, M. Trends in Aerosol Radiative Effects over China and Japan Inferred from Observed Cloud Cover, Solar “Dimming,” and Solar “Brightening”. *J. Geophys. Res. Atmos.* **2009**, *114*, D00D15. [\[CrossRef\]](#)

26. Ohmura, A. Observed Decadal Variations in Surface Solar Radiation and Their Causes. *J. Geophys. Res. Atmos.* **2009**, *114*, D00D05. [[CrossRef](#)]
27. Badarinath, K.V.S.; Sharma, A.R.; Kaskaoutis, D.G.; Kharol, S.K.; Kambezidis, H.D. Solar Dimming over the Tropical Urban Region of Hyderabad, India: Effect of Increased Cloudiness and Increased Anthropogenic Aerosols. *J. Geophys. Res. Atmos.* **2010**, *115*, D21208. [[CrossRef](#)]
28. Kambezidis, H.D. The Solar Radiation Climate of Greece. *Climate* **2021**, *9*, 183. [[CrossRef](#)]
29. Easterling, D.R.; Wehner, M.F. Is the Climate Warming or Cooling? *Geophys. Res. Lett.* **2009**, *36*, L08706. [[CrossRef](#)]
30. Foster, G.; Rahmstorf, S. Global Temperature Evolution 1979–2010. *Environ. Res. Lett.* **2011**, *6*, 044022. [[CrossRef](#)]
31. Kosaka, Y.; Xie, S.-P. Recent Global-Warming Hiatus Tied to Equatorial Pacific Surface Cooling. *Nature* **2013**, *501*, 403–407. [[CrossRef](#)]
32. Haywood, J.M.; Bellouin, N.; Jones, A.; Boucher, O.; Wild, M.; Shine, K.P. The Roles of Aerosol, Water Vapor and Cloud in Future Global Dimming/Brightening. *J. Geophys. Res. Atmos.* **2011**, *116*, D20203. [[CrossRef](#)]
33. Ruckstuhl, C.; Norris, J.R. How Do Aerosol Histories Affect Solar “Dimming” and “Brightening” over Europe?: IPCC-AR4 Models versus Observations. *J. Geophys. Res. Atmos.* **2009**, *114*, D00D04. [[CrossRef](#)]
34. Hatzianastassiou, N.; Papadimas, C.D.; Matsoukas, C.; Pavlakis, K.; Fotiadi, A.; Wild, M.; Vardavas, I. Recent Regional Surface Solar Radiation Dimming and Brightening Patterns: Inter-Hemispherical Asymmetry and a Dimming in the Southern Hemisphere. *Atmos. Sci. Lett.* **2012**, *13*, 43–48. [[CrossRef](#)]
35. Pinker, R.T.; Zhang, B.; Dutton, E.G. Do Satellites Detect Trends in Surface Solar Radiation? *Science* **2005**, *308*, 850–854. [[CrossRef](#)]
36. Hinkelman, L.M.; Stackhouse, P.W., Jr.; Wielicki, B.A.; Zhang, T.; Wilson, S.R. Surface Insolation Trends from Satellite and Ground Measurements: Comparisons and Challenges. *J. Geophys. Res. Atmos.* **2009**, *114*, D00D20. [[CrossRef](#)]
37. Zhang, X.; Liang, S.; Wild, M.; Jiang, B. Analysis of Surface Incident Shortwave Radiation from Four Satellite Products. *Remote Sens. Environ.* **2015**, *165*, 186–202. [[CrossRef](#)]
38. Wang, Z.; Zhang, M.; Wang, L.; Qin, W. A Comprehensive Research on the Global All-Sky Surface Solar Radiation and Its Driving Factors during 1980–2019. *Atmos. Res.* **2022**, *265*, 105870. [[CrossRef](#)]
39. Zhang, X.; Liang, S.; Wang, G.; Yao, Y.; Jiang, B.; Cheng, J. Evaluation of the Reanalysis Surface Incident Shortwave Radiation Products from NCEP, ECMWF, GSFC, and JMA Using Satellite and Surface Observations. *Remote Sens.* **2016**, *8*, 225. [[CrossRef](#)]
40. Kistler, R.; Kalnay, E.; Collins, W.; Saha, S.; White, G.; Woollen, J.; Chelliah, M.; Ebisuzaki, W.; Kanamitsu, M.; Kousky, V.; et al. The NCEP–NCAR 50-Year Reanalysis: Monthly Means CD-ROM and Documentation. *Bull. Am. Meteorol. Soc.* **2001**, *82*, 247–268. [[CrossRef](#)]
41. Hersbach, H.; Bell, B.; Berrisford, P.; Hirahara, S.; Horányi, A.; Muñoz-Sabater, J.; Nicolas, J.; Peubey, C.; Radu, R.; Schepers, D.; et al. The ERA5 Global Reanalysis. *Q. J. R. Meteorol. Soc.* **2020**, *146*, 1999–2049. [[CrossRef](#)]
42. Kobayashi, S.; Ota, Y.; Harada, Y.; Ebata, A.; Moriya, M.; Onoda, H.; Onogi, K.; Kamahori, H.; Kobayashi, C.; Endo, H.; et al. The JRA-55 reanalysis: General specifications and basic characteristics. *J. Meteorol. Soc. Jpn.* **2015**, *93*, 5–48. [[CrossRef](#)]
43. Slivinski, L.C.; Compo, G.P.; Whitaker, J.S.; Sardeshmukh, P.D.; Giese, B.S.; McColl, C.; Allan, R.; Yin, X.; Vose, R.; Titchner, H.; et al. Towards a More Reliable Historical Reanalysis: Improvements for Version 3 of the Twentieth Century Reanalysis System. *Q. J. R. Meteorol. Soc.* **2019**, *145*, 2876–2908. [[CrossRef](#)]
44. Hinkelman, L.M. The Global Radiative Energy Budget in MERRA and MERRA-2: Evaluation with Respect to CERES EBAF Data. *J. Clim.* **2019**, *32*, 1973–1994. [[CrossRef](#)]
45. Chakraborty, T.; Lee, X. Large Differences in Diffuse Solar Radiation among Current-Generation Reanalysis and Satellite-Derived Products. *J. Clim.* **2021**, *34*, 6635–6650. [[CrossRef](#)]
46. Jia, B.; Xie, Z.; Dai, A.; Shi, C.; Chen, F. Evaluation of Satellite and Reanalysis Products of Downward Surface Solar Radiation over East Asia: Spatial and Seasonal Variations. *J. Geophys. Res. Atmos.* **2013**, *118*, 3431–3446. [[CrossRef](#)]
47. Zhang, X.; Lu, N.; Jiang, H.; Yao, L. Evaluation of Reanalysis Surface Incident Solar Radiation Data in China. *Sci. Rep.* **2020**, *10*, 3494. [[CrossRef](#)]
48. Zhao, L.; Lee, X.; Liu, S. Correcting Surface Solar Radiation of Two Data Assimilation Systems against FLUXNET Observations in North America. *J. Geophys. Res. Atmos.* **2013**, *118*, 9552–9564. [[CrossRef](#)]
49. Boilley, A.; Wald, L. Comparison between Meteorological Re-Analyses from ERA-Interim and MERRA and Measurements of Daily Solar Irradiation at Surface. *Renew. Energy* **2015**, *75*, 135–143. [[CrossRef](#)]
50. Trolliet, M.; Walawender, J.P.; Bourlès, B.; Boilley, A.; Trentmann, J.; Blanc, P.; Lefèvre, M.; Wald, L. Downwelling Surface Solar Irradiance in the Tropical Atlantic Ocean: A Comparison of Re-Analyses and Satellite-Derived Data Sets to PIRATA Measurements. *Ocean Sci.* **2018**, *14*, 1021–1056. [[CrossRef](#)]
51. Sianturi, Y.; Marjuki; Sartika, K. Evaluation of ERA5 and MERRA2 Reanalyses to Estimate Solar Irradiance Using Ground Observations over Indonesia Region. *AIP Conf. Proc.* **2020**, *2223*, 020002. [[CrossRef](#)]
52. Tahir, Z.U.R.; Azhar, M.; Mumtaz, M.; Asim, M.; Moenuddin, G.; Sharif, H.; Hassan, S. Evaluation of the Reanalysis Surface Solar Radiation from NCEP, ECMWF, NASA, and JMA Using Surface Observations for Balochistan, Pakistan. *J. Renew. Sustain. Energy* **2020**, *12*, 023703. [[CrossRef](#)]
53. Urraca, R.; Huld, T.; Gracia-Amillo, A.; Martinez-de-Pison, F.J.; Kaspar, F.; Sanz-Garcia, A. Evaluation of Global Horizontal Irradiance Estimates from ERA5 and COSMO-REA6 Reanalyses Using Ground and Satellite-Based Data. *Sol. Energy* **2018**, *164*, 339–354. [[CrossRef](#)]

54. Babar, B.; Graversen, R.; Boström, T. Solar Radiation Estimation at High Latitudes: Assessment of the CMSAF Databases, ASR and ERA5. *Sol. Energy* **2019**, *182*, 397–411. [[CrossRef](#)]
55. Fu, L.; Bian, L.; Xiao, C. Evaluation of the Applicability of Four Reanalyzed Radiometric Data in the East Antarctic Plateau. *Chin. J. Polar Res.* **2015**, *27*, 56–64. [[CrossRef](#)]
56. Yue, K. *Influence of Aerosol Optical Depth on Solar Radiation in Yangtze River Delta*; Nanjing University of Information Science and Technology: Nanjing, China, 2016.
57. Slater, A.G. Surface Solar Radiation in North America. *J. Hydrometeorol.* **2016**, *17*, 401–420. [[CrossRef](#)]
58. Doddy Clarke, E.; Griffin, S.; McDermott, F.; Monteiro Correia, J.; Sweeney, C. Which Reanalysis Dataset Should We Use for Renewable Energy Analysis in Ireland? *Atmosphere* **2021**, *12*, 624. [[CrossRef](#)]
59. Mabasa, B.; Lysko, M.D.; Moloi, S.J. Validating Hourly Satellite Based and Reanalysis Based Global Horizontal Irradiance Datasets over South Africa. *Geomatics* **2021**, *1*, 429–449. [[CrossRef](#)]
60. Stettz, S.; Zaitchik, B.F.; Ademe, D.; Musie, S.; Simane, B. Estimating Variability in Downwelling Surface Shortwave Radiation in a Tropical Highland Environment. *PLoS ONE* **2019**, *14*, e0211220. [[CrossRef](#)]
61. Troy, T.J.; Wood, E.F. Comparison and Evaluation of Gridded Radiation Products across Northern Eurasia. *Environ. Res. Lett.* **2009**, *4*, 045008. [[CrossRef](#)]
62. Wild, M.; Schmucki, E. Assessment of Global Dimming and Brightening in IPCC-AR4/CMIP3 Models and ERA40. *Clim. Dyn.* **2011**, *37*, 1671–1688. [[CrossRef](#)]
63. Yang, D.; Bright, J.M. Worldwide Validation of 8 Satellite-Derived and Reanalysis Solar Radiation Products: A Preliminary Evaluation and Overall Metrics for Hourly Data over 27 Years. *Spec. Issue Grid Integr.* **2020**, *210*, 3–19. [[CrossRef](#)]
64. Peng, X.; She, J.; Zhang, S.; Tan, J.; Li, Y. Evaluation of Multi-Reanalysis Solar Radiation Products Using Global Surface Observations. *Atmosphere* **2019**, *10*, 42. [[CrossRef](#)]
65. Feng, F.; Wang, K. Determining Factors of Monthly to Decadal Variability in Surface Solar Radiation in China: Evidences From Current Reanalyses. *J. Geophys. Res. Atmos.* **2019**, *124*, 9161–9182. [[CrossRef](#)]
66. Jiang, H.; Yang, Y.; Wang, H.; Bai, Y.; Bai, Y. Surface Diffuse Solar Radiation Determined by Reanalysis and Satellite over East Asia: Evaluation and Comparison. *Remote Sens.* **2020**, *12*, 1387. [[CrossRef](#)]
67. Wang, K.; Ma, Q.; Li, Z.; Wang, J. Decadal Variability of Surface Incident Solar Radiation over China: Observations, Satellite Retrievals, and Reanalyses. *J. Geophys. Res. Atmos.* **2015**, *120*, 6500–6514. [[CrossRef](#)]
68. Zhou, Z.; Lin, A.; Wang, L.; Qin, W.; Zhong, Y.; He, L. Trends in Downward Surface Shortwave Radiation from Multi-Source Data over China during 1984–2015. *Int. J. Climatol.* **2020**, *40*, 3467–3485. [[CrossRef](#)]
69. You, Q.; Sanchez-Lorenzo, A.; Wild, M.; Folini, D.; Fraedrich, K.; Ren, G.; Kang, S. Decadal Variation of Surface Solar Radiation in the Tibetan Plateau from Observations, Reanalysis and Model Simulations. *Clim. Dyn.* **2013**, *40*, 2073–2086. [[CrossRef](#)]
70. Perdigão, J.C.; Salgado, R.; Costa, M.J.; Dasari, H.P.; Sanchez-Lorenzo, A. Variability and Trends of Downward Surface Global Solar Radiation over the Iberian Peninsula Based on ERA-40 Reanalysis. *Int. J. Climatol.* **2016**, *36*, 3917–3933. [[CrossRef](#)]
71. Galanaki, E.; Emmanouil, G.; Lagouvardos, K.; Kotroni, V. Long-Term Patterns and Trends of Shortwave Global Irradiance over the Euro-Mediterranean Region. *Atmosphere* **2021**, *12*, 1431. [[CrossRef](#)]
72. Zuluaga, C.F.; Avila-Diaz, A.; Justino, F.B.; Wilson, A.B. Climatology and Trends of Downward Shortwave Radiation over Brazil. *Atmos. Res.* **2021**, *250*, 105347. [[CrossRef](#)]
73. Wohland, J.; Brayshaw, D.; Bloomfield, H.; Wild, M. European Multidecadal Solar Variability Badly Captured in All Centennial Reanalyses except CERA20C. *Environ. Res. Lett.* **2020**, *15*, 104021. [[CrossRef](#)]
74. Jiao, B.; Li, Q.; Sun, W.; Martin, W. Uncertainties in the Global and Continental Surface Solar Radiation Variations: Inter-Comparison of in-Situ Observations, Reanalyses, and Model Simulations. *Clim. Dyn.* **2022**, *59*, 2499–2516. [[CrossRef](#)]
75. Randles, C.A.; Da Silva, A.M.; Buchard, V.; Colarco, P.R.; Darmenov, A.; Govindaraju, R.; Smirnov, A.; Holben, B.; Ferrare, R.; Hair, J.; et al. The MERRA-2 Aerosol Reanalysis, 1980—Onward, Part I: System Description and Data Assimilation Evaluation. *J. Clim.* **2017**, *30*, 6823–6850. [[CrossRef](#)]
76. The Second Modern-Era Retrospective Analysis for Research and Applications (MERRA-2). Available online: <http://disc.sci.gsfc.nasa.gov/mdisc/> (accessed on 30 August 2022).
77. Gelaro, R.; McCarty, W.; Suárez, M.J.; Todling, R.; Molod, A.; Takacs, L.; Randles, C.A.; Darmenov, A.; Bosilovich, M.G.; Reichle, R.; et al. The Modern-Era Retrospective Analysis for Research and Applications, Version 2 (MERRA-2). *J. Clim.* **2017**, *30*, 5419–5454. [[CrossRef](#)]
78. Chou, M.D.; Suarez, M.J. *A Solar Radiation Parameterization (CLIRAD-SW) for Atmospheric Studies*; NASA Technical Memorandum NASA/TM-1999-104606, 40; NASA Goddard Space Flight Center: Greenbelt, MD, USA, 1999.
79. Joseph, J.H.; Wiscombe, W.J.; Weinman, J.A. The Delta-Eddington Approximation for Radiative Flux Transfer. *J. Atmos. Sci.* **1976**, *33*, 2452–2459. [[CrossRef](#)]
80. Loeb, N.G.; Doelling, D.R.; Wang, H.; Su, W.; Nguyen, C.; Corbett, J.G.; Liang, L.; Mitrescu, C.; Rose, F.G.; Kato, S. Clouds and the Earth’s Radiant Energy System (CERES) Energy Balanced and Filled (EBAF) Top-of-Atmosphere (TOA) Edition-4.0 Data Product. *J. Clim.* **2018**, *31*, 895–918. [[CrossRef](#)]
81. Loeb, N.G.; Priestley, K.J.; Kratz, D.P.; Geier, E.B.; Green, R.N.; Wielicki, B.A.; Hinton, P.O.; Nolan, S.K. Determination of Unfiltered Radiances from the Clouds and the Earth’s Radiant Energy System Instrument. *J. Appl. Meteorol.* **2001**, *40*, 822–835. [[CrossRef](#)]

82. Su, W.; Corbett, J.; Eitzen, Z.; Liang, L. Next-Generation Angular Distribution Models for Top-of-Atmosphere Radiative Flux Calculation from CERES Instruments: Methodology. *Atmos. Meas. Tech.* **2015**, *8*, 611–632. [CrossRef]
83. Doelling, D.R.; Loeb, N.G.; Keyes, D.F.; Nordeen, M.L.; Morstad, D.; Nguyen, C.; Wielicki, B.A.; Young, D.F.; Sun, M. Geostationary Enhanced Temporal Interpolation for CERES Flux Products. *J. Atmos. Ocean. Technol.* **2013**, *30*, 1072–1090. [CrossRef]
84. CERES Data Products. Available online: <https://ceres.larc.nasa.gov/Data> (accessed on 30 August 2022).
85. Michalsky, J.; Dutton, E.; Rubes, M.; Nelson, D.; Stoffel, T.; Wesely, M.; Splitt, M.; Deluisi, J. Optimal Measurement of Surface Shortwave Irradiance Using Current Instrumentation. *J. Atmos. Ocean Technol.* **1999**, *16*, 55–69. [CrossRef]
86. Wild, M.; Folini, D.; Schär, C.; Loeb, N.; Dutton, E.G.; König-Langlo, G. The Global Energy Balance from a Surface Perspective. *Clim. Dyn.* **2013**, *40*, 3107–3134. [CrossRef]
87. Global Energy Balance Archive. Available online: <https://geba.ethz.ch/> (accessed on 30 August 2022).
88. Wild, M.; Folini, D.; Schär, C.; Loeb, N.; Dutton, E.G.; König-Langlo, G. Basic Measurements of Radiation from the Baseline Surface Radiation Network (BSRN) in the Years 1992 to 2012, Reference List of 6378 Datasets. 2013.
89. World Radiation Monitoring Center (WRMC) Baseline Surface Radiation Network (BSRN). Available online: <https://bsrn.awi.de/data/> (accessed on 30 August 2022).
90. Ohring, G.; Romanov, P.; Ferraro, R.; Heidinger, A.; Laszlo, I.; Zou, C.-Z.; Foster, M. Satellite Observations of North American Climate Change. In *Climate Change in North America*; Ohring, G., Ed.; Springer International Publishing: Cham, Switzerland, 2014; pp. 95–165, ISBN 978-3-319-03768-4.
91. Stocker, T.F.; Qin, D.; Plattner, G.K.; Tignor, M.M.; Allen, S.K.; Boschung, J.; Nauels, A.; Xia, Y.; Bex, V.; Midgley, P.M. Climate Change 2013: The Physical Science Basis. In *Contribution of Working Group I to the Fifth Assessment Report of the Intergovernmental Panel on Climate Change*; Cambridge University Press: Cambridge, UK; New York, NY, USA, 2014.
92. Theil, H. A Rank-Invariant Method of Linear and Polynomial Regression Analysis. In *Henri Theil's Contributions to Economics and Econometrics: Econometric Theory and Methodology*; Raj, B., Koerts, J., Eds.; Springer: Dordrecht, The Netherlands, 1992; pp. 345–381, ISBN 978-94-011-2546-8.
93. Sen, P.K. Estimates of the Regression Coefficient Based on Kendall's Tau. *J. Am. Stat. Assoc.* **1968**, *63*, 1379–1389. [CrossRef]
94. Mann, H.B. Nonparametric Tests against Trend. *Econometrica* **1945**, *13*, 245–259. [CrossRef]
95. Kendall, M.G. *Rank Correlation Methods*, 4th ed.; Charles Griffin: London, UK, 1975.
96. Wang, Y.; Trentmann, J.; Yuan, W.; Wild, M. Validation of CM SAF CLARA-A2 and SARA-E Surface Solar Radiation Datasets over China. *Remote Sens.* **2018**, *10*, 1977. [CrossRef]
97. Baker, M.B.; Peter, T. Small-Scale Cloud Processes and Climate. *Nature* **2008**, *451*, 299–300. [CrossRef]
98. Stensrud, D.J. *Parameterization Schemes: Keys to Understanding Numerical Weather Prediction Models*; Cambridge University Press: Cambridge, UK, 2007.
99. Cullather, R.I.; Bosilovich, M.G. The Energy Budget of the Polar Atmosphere in MERRA. *J. Clim.* **2012**, *25*, 5–24. [CrossRef]
100. Xia, X.A.; Wang, P.C.; Chen, H.B.; Liang, F. Analysis of Downwelling Surface Solar Radiation in China from National Centers for Environmental Prediction Reanalysis, Satellite Estimates, and Surface Observations. *J. Geophys. Res. Atmos.* **2006**, *111*, D09103. [CrossRef]
101. Ma, Q.; Wang, K.; Wild, M. Impact of Geolocations of Validation Data on the Evaluation of Surface Incident Shortwave Radiation from Earth System Models. *J. Geophys. Res. Atmos.* **2015**, *120*, 6825–6844. [CrossRef]
102. Korras-Carraca, M.-B.; Gkikas, A.; Matsoukas, C.; Hatzianastassiou, N. Global Clear-Sky Aerosol Speciated Direct Radiative Effects over 40 Years (1980–2019). *Atmosphere* **2021**, *12*, 1254. [CrossRef]
103. Ramanathan, V.; Ramana, M.V.; Roberts, G.; Kim, D.; Corrigan, C.; Chung, C.; Winker, D. Warming Trends in Asia Amplified by Brown Cloud Solar Absorption. *Nature* **2007**, *448*, 575–578. [CrossRef]
104. Ruckstuhl, C.; Philipona, R.; Behrens, K.; Collaud Coen, M.; Dürr, B.; Heimo, A.; Mätzler, C.; Nyeki, S.; Ohmura, A.; Vuilleumier, L.; et al. Aerosol and Cloud Effects on Solar Brightening and the Recent Rapid Warming. *Geophys. Res. Lett.* **2008**, *35*, L12708. [CrossRef]
105. NOAA National Centers for Environmental Information. *Climate at a Glance: Global Mapping 2022*; NOAA National Centers for Environmental Information: Washington, DC, USA, 2022.
106. Sanchez-Lorenzo, A.; Wild, M.; Brunetti, M.; Guijarro, J.A.; Hakuba, M.Z.; Calbó, J.; Mystakidis, S.; Bartok, B. Reassessment and Update of Long-Term Trends in Downward Surface Shortwave Radiation over Europe (1939–2012). *J. Geophys. Res. Atmos.* **2015**, *120*, 9555–9569. [CrossRef]
107. Padma Kumari, B.; Goswami, B.N. Seminal Role of Clouds on Solar Dimming over the Indian Monsoon Region. *Geophys. Res. Lett.* **2010**, *37*, L06703. [CrossRef]